ELECTRICAL PROPERTIES OF NEUTRON-
TRANSMUTATION-DOPED GERMANIUM

Marilyn Rodder

Department of Materials Science and Mineral Engineering and
Department of Instrument of Science and Engineering
Lawrence Berkeley Laboratory, University of California
Berkeley, California 94720

DISCLAIMER

August 1982

MASTER

ACKNOWLEDGMENTS

TABLE OF CONTENTS

ELECTRICAL PROPERTIES OF NEUTRON-
TRANSMUTATION-DOPED GERMANIUM

Marilyn Rodder

Department of Materials Science and Mineral Engineering and
Department of Instrument Science and Engineering,
Lawrence Berkeley Laboratory, University of California
Berkeley, California 94720

Abstract

Electrical properties of neutron-transmutation-doped germanium (NTD Ge) and nearly uncompensated gallium-doped germanium have been measured as functions of net-impurity concentration ($2 \times 10^{15} \mathrm{cm}^{-3} \leq N_A - N_D \leq 5 \times 10^{16} \mathrm{cm}^{-3}$) and temperature ($0.3 \, \mathrm{K} \leq T \leq 300 \, \mathrm{K}$).

The method of impurity conduction as a function of carrier concentration and compensation was investigated in the low temperature hopping regime. For nearest neighbor hopping, the resistivity is expected to vary as $\rho = \rho_0 \exp(\Delta/T)$ while Mott's theory of variable range hopping predicts that $\rho = \rho_0 \exp(\Delta/T)^{1/4}$ in the low temperature limit. In contrast, our results show that the resistivity can best be approximated by $\rho = \rho_0 \exp(\Delta/T)^{1/2}$ in the hopping regime down to 0.3 K.

1. Background

1.1 Introduction

Although semiconductors have been studied for many years, they actually became popular only after Schockley, Bardeen and Brattain invented the transistor[1] in 1947. Because of this invention, research and development of semiconductors was heavily pursued. Their most direct uses take advantage of their unique electrical behavior, as in transistors, amplifiers and memory devices. Other applications include those which combine electrical and optical effects such as sensing devices, for example, in strain gauges, nuclear radiation sensing devices and low temperature semiconducting bolometers used for detection of far infrared radiation.

1.2 Crystal Structure

Semiconductors are extremely versatile in their applications because their electrical conductivities range from metallic to insulating depending on temperature and doping. Besides the elemental semiconductors, Si and Ge, there are many compound semiconductors such as GaAs, GaP and InSb. Ternary and quaternary compound semiconductors are becoming very important for solid state lasers, photodiodes and light-emitting diodes. The elemental semiconductors (Group IV) all crystallize in the diamond structure, in which each atom is surrounded by four covalently bonded neighboring atoms, forming a regular tetrahedron as shown in Fig. 1a. The Group III-V compounds crystallize in the zincblende structure. Thus in GaAs, each Ga atom is heteropolarly surrounded by four As atoms as in Fig. 1b.
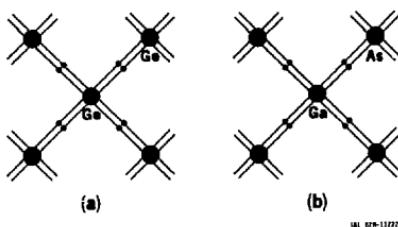
Fig. 1. Tetrahedral bonds in Ge and GaAs. Black dots represent coval-
ently bonded electrons.

1.3 Energy Bands

Electrical conduction in crystalline solids--semiconduction--can
be understood quantitatively in terms of energy bands, that is, elec-
tron energies versus k-space. A common method of describing electron
energies is to use a model which starts with a free assembly of elec-
trons[2], and then to consider the changes in their movement resulting
from the restrictions presented by the crystal lattice.

First, consider a free electron in space. The time independent
Schrodinger equation for the free electron is:

$$\nabla^2 \psi = (-2mE/\hbar^2)$$ (1.1)

where ψ is the wave function, and E is the energy of the electron.
Then:

$$\bar{\psi} = A \exp(i\bar{k}\bar{r}) + B \exp(-i\bar{k}\bar{r})$$ (1.2)

where $\bar{k}$ is the wave vector describing the momentum of the electron, $\bar{r}$
is the position vector, and $|\psi|^2$ is the probability of finding the
electron anywhere in space. The energy, in the one-dimensional case
is:

$$E = (h^2/2m)k^2$$ (1.3)

as shown in Fig. 2a[3]. But unlike electrons in free space, the values
that k can have are quantized, due to the de Broglie relationship
between the electron wavelength, λ, and its momentum, p:

$$\lambda = h/p \qquad\qquad (1.4a)$$

$$p = (2mE)^{1/2} \qquad\qquad (1.4b)$$

such that k, equal to $2\pi/\lambda$ is:

$$k = (2mE)^{1/2}/h = 2\pi/\lambda. \qquad\qquad (1.4c)$$
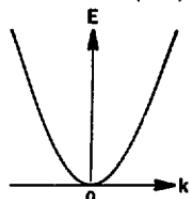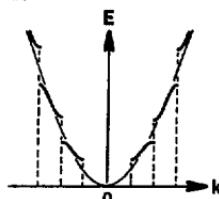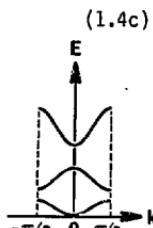
(a)   **(b)**   **(c)**

XBL 828-11223

Fig. 2. E vs. k in one dimension for (a) free electrons, (b) electrons
moving in a periodic potential, and (c) E vs. reduced wave
number. The scale of k in Fig. 2c has been expanded for visu-
al clarification.

Bloch extended this model to that of a crystal lattice in which
there is a periodically varying potential due to the charges at the
lattice sites[4], as in Fig. 3.
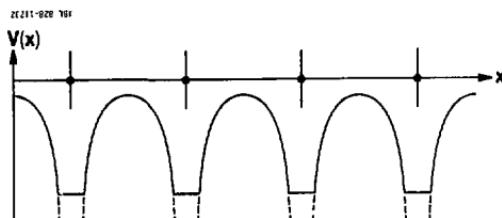
Fig. 3. The variation in crystal potential with distance between lat-
tice sites.

Bloch showed that solutions to the one-dimensional wave functions would be:

$$\Psi_k = u_k \exp(ikx) \tag{1.5a}$$

and
$$\Psi(x \pm a) = \exp(\pm ika)\Psi(x) \tag{1.5b}$$

where a is the lattice periodicity, $\exp(ikx)$ represents a plane wave and $u_k(x)$ has the same periodicity as the lattice. Thus, if there are N lattice sites and $\Psi(x + Na) = \Psi(x)$, then $\exp(ikNa) = 1$. The resulting allowed k are:

$$k = 2\pi n/Na \quad n = (0, \pm 1, \pm 2, \pm 3 \ldots). \tag{1.6}$$

This leads to discontinuities in E versus k which occur at the values $k - n\pi/a$, as shown in Fig. 2b. These discontinuities can be understood as follows. For an electron of wavelength $\lambda = 2a$ such that $k = \pi/a$, we have the condition of Bragg reflection. Such an electron can no longer be represented as a traveling wave. Instead, it should be represented as a standing wave comprised of two waves, $\exp(ikx)$ and $\exp(-ikx)$, which travel in opposite directions. The summation of the two waves leads to two solutions of different allowed energies at $k = \pi/a$. The allowed energy states thus fall into bands separated by forbidden gaps.

If the energy of a state is described in terms of a reduced wave number restricted to the range $-\pi/a \leq k \leq \pi/a$, and a quantum number to describe the band to which the state belongs, then the band structure will have the form in Fig. 2c. In order to describe the electron energies as a function of k, one defines the effective mass m^*:

$$m^* = h^2/(d^2E/dk^2) \tag{1.7a}$$

and
$$E = (h^2/2m^*)k^2 \tag{1.7b}$$

The inverse value of the effective mass is the curvature in the E versus k dependence shown in Fig. 2c.

1.4 Density of States

Proceeding from the concept of quantization, a "density of states" can be introduced[5]. In three-dimensional k-space, the number of states in a volume element $dk = dk_x dk_y dk_z$ is:

$$(L^3)dk/8\pi^3 \tag{1.8}$$

where we consider a cubic volume of side L and $k = 2\pi n/L$ (n = $0, \pm 1, \pm 2, \ldots$). Then, the number of states between k and $(k + dk)$ is:

$$(L^3)(4\pi k^2)dk/8\pi^3. \tag{1.9}$$

The density of states per unit energy range and volume, for given spin direction, is N(E). For a volume $L^3 = 1$,

$$N(E) = 4\pi k^2 dk/8\pi^3. \tag{1.10}$$

Since $E = h^2 k^2/2m^*$, the density of states is then

$$N(E) = 1/4\pi^2)(2m^*/h^2)^{3/2}\sqrt{E} \tag{1.11}$$

The concentration of electrons per unit volume can be found by integrating over the density of states Fermi distribution product. The Fermi-Dirac distribution function is defined by[3]:

$$f(E) = [\exp\left\{(E - E_F)/kT\right\} + 1]^{-1} \tag{1.12}$$

where f(E) is the probability that a state of energy E is occupied, E_F is the Fermi energy, k is Boltzmann's constant, and T is the absolute temperature. E_F is the energy value which is defined at absolute zero temperature so that the integral over N(E) and f(E), up

to E_F equals the number of all the electrons, n, per unit volume E_F is
given by[4]:

$$2\int^{E_F} N(E)dE = n \tag{1.13}$$

The number of electrons in each orbital state can be two, one for each
spin direction, which leads to the factor 2 before the integral. $f(E)$
versus E is shown in Fig. 4.
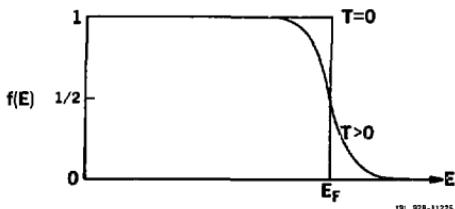
Fig. 4. The Fermi-Dirac distribution function versus the energy of an
electron state. At $T = 0$, $f = 1$ for $E < E_F$ and $f = 0$ for
$E > E_F$, so that all the electrons fall into the lowest
energy states. For $T > 0$, the distribution function is
exactly $1/2$ at $E = E_F$.

1.5 Intrinsic Semiconduction

From the previous section, we know that current cannot flow in a
pure semiconductor at zero temperature because all the states below
E_F are filled, with no unoccupied states for electrons to flow.
However, for $T > 0$, an electron can be freed from the covalent bond by
means of thermal excitation. This creates both a conducting electron
and a hole, which can be thought of as a positively charged particle
whose motion results from a shift of a valence electron. Under an
applied field, the motion of electrons and holes is in opposite direc-
tions giving rise to electrical conductivity. Thus, we have "intrin-
sic" semiconduction in a pure semiconductor.

The energies of electrons and holes can be described in terms of the energy bands of section 1.3. The "valence band" is defined as the highest occupied band at $T = 0$, and the "conduction band" is the lowest unoccupied band at $T = 0$. Thus, the energy necessary to free an electron from a bond is given by the energy gap, E_G, between the two bands. For $T > 0$ then, those electrons with enough energy to cross the forbidden energy gap will conduct in the lowest available conduction band states, whereas the holes conduct in the valence band, as in Fig. 5.

XBL 828-11226
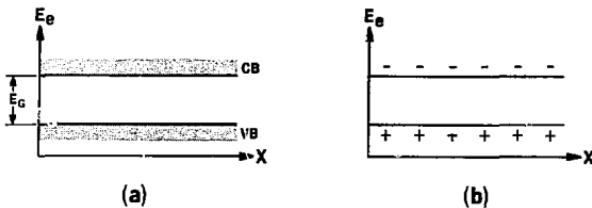
Fig. 5. Intrinsic semiconductor (a) at low temperatures and (b) at higher temperature where electrons can be excited across the bandgap.

A second way to excite electrons across the bandgap is by photon absorption. If the light is of a wavelength such that $h\nu > E_G$, electron-hole pairs will be generated, and photoconduction will occur.

The concentration of electrons n and holes p in thermal semiconduction is dominated by generation and recombination. At equilibrium, the following relationship holds[3]:

$$n + p \rightleftharpoons (np) \tag{1.14}$$

where (np) refers to the unexcited state, or recombination. For n and p small compared to the number of states in the crystal, thermodynamics predicts:

$$np = K \tag{1.15}$$

where K is a function of temperature only. Then, by defining
$n = p = n_i$, we have for intrinsic material:

$$np = n_i^2. \tag{1.16}$$

Using Eq. 1.12 one can approximate $f(E)$, the so-called "Boltzmann tail"
for $(E - E_F) \gg kT$, to be:

$$f(E) = \exp[(E_F - E)/kT]. \tag{1.17}$$

Using this result and Eq. 1.11, we have:

$$n = n_i = \int f(E)N(E)dE = N_c \exp[(E_F - E_c)/kT] \tag{1.18a}$$

for $\qquad N_c = 2(2\pi m_e^* kT/h^2)^{3/2} \tag{1.18b}$

where n is the concentration of electrons and N_c is the density of
states in the conduction band (CB). Similarly, the concentration of
holes in the valence band (VB) is:

$$p = N_v \exp[(E_v - E_F)/kT] \tag{1.19a}$$

for $\qquad N_v = 2(2\pi m_h^* kT/h^2)^{3/2} \tag{1.19b}$

where N_v is the density of states in the valence band. Combining
Eqs. 1.18a and 1.19a, we have for the intrinsic concentration:

$$n_i^2 = N_c N_v \exp(-E_G/kT). \tag{1.20}$$

1.6 Extrinsic Semiconduction

The discussion of conduction in section 1.5 applies to a pure
semiconductor. In most applications, however, semiconductors are
doped with impurities which supply most of the carriers, thereby pro-
viding "extrinsic" semiconduction. Typical technologically important
concentrations range from $10^{10} cm^{-3}$ to more than $10^{20} cm^{-3}$.

The most commonly encountered doping concentrations lie around $10^{15}cm^{-3}$ or ~ 100 ppb, a very pure substance indeed! The most common dopants for Si and Ge are those elements of Group III and V.

1.6.1 Elemental Donors in Si and Ge - The Group V elements (As, P, Bi, Sb) have five valence electrons. Four of the electrons contri- bute to the tetrahedral bond of the host crystal (usually Group IV), while the fifth electron migrates through the crystal, as with P in a Ge crystal as shown in Fig. 6.
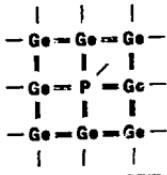
Fig. 6. Substitutional dopant atom positions in an elemental semicon-
         ductor for a donor with extra electron.

In the case of a phosphorus impurity, the impurity consists of a positive ion, P^+ binding an electron in its Coulomb field. However, the Coulomb attraction between the P^+ and a free electron is weak due to the large relative dielectric constant of the semiconductor crystal. The Coulomb potential is:

$$V(r) = -e^2/4\pi\epsilon_r\epsilon_0 r \qquad (1.21)$$

where ϵ_r is the relative dielectric constant of the medium. The values of ϵ_r for Si and Ge are 11.7 and 16.0, respectively, showing

a decrease in the interaction force. This screening is responsible
for the small binding energy of the electron at the donor site. Using
the bohr model[1], we find that this small binding energy is related
to the Bohr radius of the donor electron, a^*:

$$a^* = \hbar^2 \kappa / m^* e^2 \tag{1.22}$$

where $\kappa = 4\pi\epsilon_r\epsilon_0$. In Eq. 1.22, m^* is the effective mass, and $\hbar$ and
ϵ_0 are constants. This is essentially the result of what is called the
effective mass theory, which predicts surprisingly well both binding
energies and Bohr radii. Donors which can be described with this
simple model are called in analogy to hydrogen, "hydrogenic". A typi-
cal binding energy corresponding to the ground state of the donor in
Ge is $E_D= 0.01$ eV. This is small compared to the bandgap, E_G, which
is 0.7 eV for Ge at room temperature. As shown in Fig. 7, the level is
so close to the conduction band that almost all donors lose their elec-
trons, i.e., are ionized at room temperature.
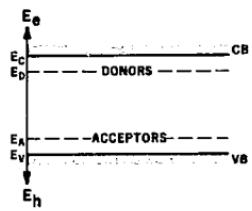
Fig. 7. Donor level position at conduction band edge, and (b) accep-
tor level position at valence band edge at room temperature.

The concentration of electrons n is for all practical purposes, equal
to the concentration of donors N_D, if $N_D \gg n_i$. From Eq. 1.16:

$$n = N_D \gg n_i \tag{1.23a}$$

$$p = n_i^2/N_D \tag{1.23b}$$

1.6.2 <u>Acceptors</u> – In order to make the host crystal conducting
with holes instead of electrons, Group III acceptors (B, Al, Ga, In)
which are trivalent impurities and which accept electrons to complete
the tetrahedral bond of the host are used. When the vacancy of the
electron bond is filled by an electron moving into the site from an-
other bond, a hole is introduced in the latter bond. The hole then
migrates throughout the crystal. The acceptor is negatively charged
since it has entrapped the additional electron. The positively charged
hole is attracted and bound by the acceptor with a small binding energy
of ~ 0.01 eV, in close analogy to the "hydrogenic" model used for
donors. Thus, essentially all the acceptors are ionized at room tem-
perature. The acceptor level lies just above the valence band edge,
as in Fig. 7. This level corresponds to the hole being captured by
the acceptor. When an acceptor is ionized (i.e., by an electron ex-
cited from the top of the valence band to fill the hole), the hole
jumps to the top of the valence band and becomes a free carrier.

That donors and acceptors lie in the bandgap does not contradict
the model described in section 1.3 because the model was for a pure
crystal. Extrinsic semiconductors contain impurity states, or imper-
fections. Furthermore, impurity states which are bound states are
localized, not delocalized as are Bloch electrons. Impurity states
are thus nonconducting.

1.6.3 <u>Compensation</u> – Compensation is the result of the presence
of both donors and acceptors and can be achieved by introducing Group
III acceptors into n-type material or Group V donors into p-type mate-
rial. Compensation K is defined as the ratio of the concentration of
minority impurities to majority impurities. Thus, in a semiconductor
with N_A acceptors and N_D donors, with $N_A > N_D$, the compensation is:

$$K = N_D/N_A \qquad (1.24)$$

The effects of compensation will be explained in chapter six.

1.7 Band Structure of Real Semiconductors

In section 1.3, a conduction band centered at $\bar{k} = 0$ was assumed.
However, the band structures of real semiconductors have regions where
the energy $E(\bar{k})$ is not quadratic in $\bar{k}$, so that those states cannot be
represented by a single effective mass introduced in section 1.3.
Figure 8a shows the band structure in germanium[5].

XBL 828-11238
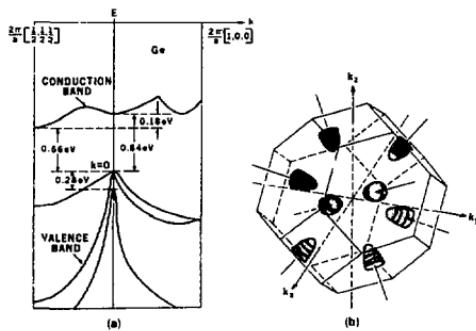
Fig. 8. (a) Band structure of Ge plotted along the [100] and [111]
         directions, and (b) ellipsoidal energy surface corresponding
         to primary valleys along the <111> directions.

The conduction band has its minimum along the [111] direction at the zone edge. Due to the cubic symmetry in the k_x-, k_y- and k_z- directions, the energy band must have tetrahedral symmetry. Thus, there are actually eight minima, shown in Fig. 8b. This modifies Eq. 1.22, so that m^* will be some average between the respective longitudinal and transverse masses of $m_1 = 1.6\ m_0$ and $m_t = 0.082\ m_0$ for germanium. This gives a value of $a = 45\ \text{Å}$ for Ge, where the dielectric constant is $k = 16$ and the lattice constant is $5.65\ \text{Å}$. This is a large radius, so that impurity orbits overlap at relatively low impurity concentrations.

Because we have eight conduction band minima in Ge, there are then eight solutions to the lowest energy state. This degeneracy is not allowed by the symmetry of the lattice; thus, corrections need to be made in calculating the effective mass for the ground state.

The behavior of an electron in a crystalline solid is determined by the Schrodinger equation[4]:

$$[-\hbar^2/2m\nabla^2 + V(\bar{r})]\psi\ (\bar{r}) = E\psi(\bar{r}) \tag{1.25}$$

where $V(\bar{r})$ is the crystal potential "seen" by the electron, and $\psi(\bar{r})$ and E are respectively, the state function and energy of the electron. If Eq. 1.25 is modified to account for the longitudinal and transverse masses, m_1 and m_t, the result for the ground state is:

$$\left\{(-\hbar^2/2m_1)\ \nabla^2(x) + (-\hbar^2/2m_t)[\nabla^2(y) + \nabla^2(z)] + V(\bar{r})\right\}\psi(\bar{r}) =$$
$$E\psi(\bar{r}). \tag{1.26}$$

It is always possible to write the solution to Eq. 1.25 as:

$$\psi(\bar{r}) = u(\bar{r})f(\bar{r}) \tag{1.27}$$

where $u(\bar{r})$ has the same symmetry as the lattice and $f(\bar{r})$ is a hydrogen–

like envelope function. It can be shown[6] that the ground state enve-
lope function $f(\bar{r})$ which satisfies Eq. 1.26 for the ground state
function is:

$$f(r) \sim \exp(-r/a^*) \qquad (1.28)$$

where $r > r_a$ and $4\pi r_a^3/3$ is the atomic volume. Equations 1.26 to 1.28
then, represent the modifications to the ground state energy states of
a donor impurity. The other singly bound energy states can be repre-
sented by Eqs. 1.25, 1.27 and 1.28.

1.8 Calculating Energy Bands: The Tight-Binding Approximation

One method used to calculate Eq. 1.25 is by the "tight-binding"
method[5]. This method assumes a crystalline array of N potential
wells, as shown.

XBL 828-11227
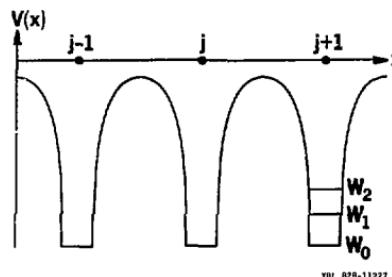
Fig. 9. The potential energy of an electron in a crystal, where W_0,
W_1 and W_2 are energy levels.

In each well, the electrons have bound states with energies W_0, W_1,
. . . W_n and wave functions ϕ_0, ϕ_1, . . . ϕ_n. When the electron moves
from one well to another, a band containing N states is formed from
each bound state of a single well. The wave function describing this
motion is:

$$\Psi_{nk} = N^{-1/2} \sum_{j=1}^{N} \exp(ikX_j)\phi_{nj}(r - X_j) \tag{1.29}$$

where X_j describes the position of the jth atom and $\phi_{nj}(r - X_j)$ is the atomic orbital centered around the jth atom. The energy of the electron described by Ψ_k is given, according to quantum mechanics[13], by:

$$E(k) = < \Psi_k |H| \Psi_k > \tag{1.30}$$

where H is the Hamiltonian of the electron. The value $E_n(k)$ of the energy of an electron with this wave function is:

$$E_n(\bar{k}) = W_n + \int (\Psi_{nk}^* \Delta V \Psi_{nk}) d^3x \tag{1.31}$$

where ΔV is the difference between the potential energy V and that of the simple well. If it is assumed that only nearest-neighbor interactions give the most significant overlap integrals, then for a simple cubic lattice with lattice constant, a:

$$E_n(\bar{k}) = W_n - \beta - 2I(\cos k_x a + \cos k_y a + \cos k_z a) \tag{1.32a}$$

where $\quad \beta = -\int |\phi_i|^2 \Delta V d^3x, \tag{1.32b}$

and I is the "overlap energy integral", where

$$I = - (\phi_{i+t}^* \Delta V \phi_i) d^3x \tag{1.32c}$$

Thus, according to the tight-binding approximation, the spread between the minimum and maximum energies of the band is proportional to the overlap integral I. The bandwidth B in this approximation is $B = 2zI$, where z is the number of nearest neighbors in the lattice[4].

1.9 Anderson Localization

The tight-binding model above assumes that the donor sites form a periodic lattice. Although the impurity sites occupy substitutional

positions of the host crystal, they have a low enough concentration
that we can regard them as randomly distributed. This is known as
lateral disorder. The value of the overlap integral I in Eq. 32c will
then change from site to site due to the random donor distribution.

Anderson[7] considered the effect of the fluctuations by consider-
ing what happens when a potential V is added to each lattice site in
the tight-binding approximation. V was allowed to lie between the
limits $\pm V_0$, as shown in Fig. 10.
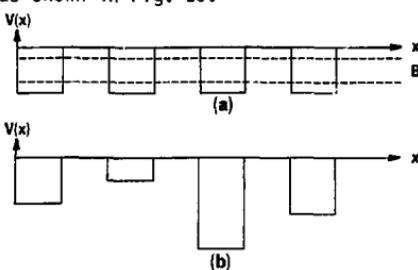
Fig. 10. One-dimensional random potential energy introduced by
Anderson for (a) $V_0 = 0$ and (b) V_0/B large.

Anderson showed that there exists a critical value (V_0/B)crit such
that the solutions to the Schrodinger equation will lead to "localized"
wave functions, where localization means that no conductivity can occur
in the lattice at absolute zero temperature. He then proved, using the
Born approximation for the mean free path, that for (V_0/B) just less
than (V_0/B)crit, the minimum value for the conductivity will be:

$$\sigma_{min} = (\pi/4z)(e^2/hd_c)\left\{(B/V_0)crit\right\}^2 \tag{1.33}$$

where d_c is the average distance between impurity centers. Calcula-
tions estimate that (V_0/B)crit = 2. The effect of disorder is to
produce localization of states, even though there may be strong over-
lap between wave functions of adjacent states.

Thus, if the Anderson criterion of $V_0 \geq 2B$ is satisfied for a particular band, all states in the band will be localized. If the Anderson criterion is not satisfied, then the states are localized in one range of energies and not localized in another where the two ranges are separated by a critical energy E_c. The effects of Anderson localization will be further discussed in Chapter 6.

2. Electrical Conduction in Doped Semiconductors

2.1 Introduction

The most fundamental electronic property of materials is electrical conductivity. Both electrons and holes contribute to electrical current. For a sample with only one type of carrier--for example, electrons--the electrical conductivity σ is defined as:

$$\sigma = ne^2 \tau_e / m_e^* \tag{2.1}$$

where τ_e is the average time between collisions of an electron. The electrical conductivity of a material depends on two factors: 1) the number of current carriers per unit volume, and 2) the mobility of the carriers under an applied field. The electrical mobility μ_e is defined as the ratio $v_e/\mathscr{E}$, the velocity per unit field strength. Since the drift velocity in the field is:

$$v_e = -e \tau_e \mathscr{E}/m_e^*, \tag{2.2a}$$

then, $\qquad \mu_e = e \tau_e / m_e^* \tag{2.2b}$

and $\qquad \sigma_e = ne\mu_e \tag{2.2c}$

Analogously, in a sample which is p-type we have the conductivity of holes σ_h:

$$\sigma_h = pe^2\tau_h/m_h^* = pe\mu_h \tag{2.3}$$

for hole mobility μ_h and average time between collisions of a hole τ_h. If there are both electrons and holes in a sample, their currents and conductivities are additive. The total conductivity σ is:

$$\sigma = \sigma_e + \sigma_h \tag{2.4}$$

A second commonly used parameter is the resistivity ρ:

$$\rho = 1/\sigma = 1/ne\mu_e \quad \text{(for n-type)} \tag{2.5a}$$

$$= 1/pe\mu_h \quad \text{(for p-type)} \tag{2.5b}$$

2.2 Temperature Dependence of the Conductivity: Low Concentration $(<10^{15}\text{cm}^{-3})$

The temperature dependences of the resistivity and carrier concentration of semiconductors doped with low impurity concentrations $(\sim 10^{14}\text{cm}^{-3})$ are shown in Figs. 11a and 11b. The resistivity changes with temperature primarily as a result of the change in carrier concentration n. At temperatures far above room temperature, there is appreciable intrinsic carrier concentration, and ln n will vary inversely to the temperature with a slope of $(-E_G/2k)$, as seen from Eq. 1.20. The $T^{3/2}$ dependence of N_c in Eq. 1.18b is generally small compared to the exponential dependence of T in Eq. 1.18a. As the temperature decreases, the thermal energy of the intrinsic carriers decreases, such that their concentration decreases and the resistivity increases. This is shown in segment 1 of Figs. 11a and 11b.
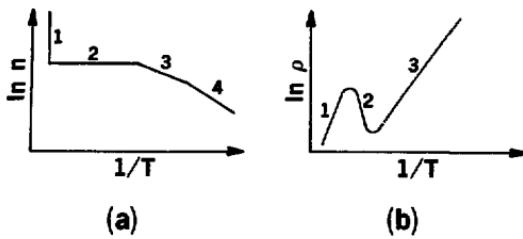
XBL 828-11228

Fig. 11. (a) Carrier concentration and (b) resistivity relationships
          as a function of temperature.

At about room temperature, extrinsic impurity conduction dominates and
there is complete ionization of donors (in n-type material) or acceptors
(in p-type material). Thus, in segment 2 of Fig. 11a, we find:
$n = \left| N_D - N_A \right|$ in the extrinsic region. The drop in resistivity in
this range is due to the temperature dependence of the mobility μ. The
carrier mobility increases with decreasing temperature due to a decrease
in "lattice scattering". Lattice vibrations lead to shorter mean free
paths for carriers and carriers travel faster at higher temperatures, thus
shortening the time between collisions. Both factors decrease the mobil-
ity at high temperatures.

As the temperature drops below about 100 K, the carriers begin to
freeze out on the donor/acceptor centers in n-type/p-type material. The
free carrier concentration then drops, as in segment 3 of Fig. 11a and the
resistivity correspondingly increases. The slopes of segments 3 and 4 in
the freeze-out region of the concentration curve are described by approxi-
mations[3]. Consider, for example, and n-type semiconductor ($N_D > N_A$).
Charge neutrality requires that:

$$n + (N_A - p_A) = p + (N_D - n_D)$$

where N_A and N_D are the total concentrations of acceptor and donor
centers; and p_A and n_D are the concentrations of holes and electrons

on centers. Thus, the concentration of electrons in donor centers is $n_D = N_D f(E_D)$. The rate of loss of electrons from donor centers to the conduction band is:

$$k_1 N_C (N_D - N_A - n) \tag{2.7}$$

where N_C is the number of empty conduction band states, $(N_D - N_A - n)$ is the number of filled, or neutral, donors and k_1 is a proportionality constant. The rate of return of electrons to the donors is:

$$k_2 n(n + N_A). \tag{2.8}$$

At equilibrium,

$$n(n + N_A)/N_C(N_D - N_A - n) = k_1/k_2 = K \tag{2.9a}$$

and $$K = \exp(E_D - E_C)/kT \tag{2.9b}$$

For $n \gg N_A$, and $n < N_D$, Eq. 2.9a reduces to:

$$n = (N_C N_D)^{1/2} \exp(E_D - E_C)/2kT \tag{2.10}$$

while for $n \ll N_A$,

$$n = N_C[(N_D - N_A)/N_A]\exp(E_D - E_C)/kT \tag{2.11}$$

Equation 2.10 applies to segment 3 of the ln n versus T^{-1} curve where $n > N_A$ and n $(E_D - E_C)/2kT$. As n decreases to $n < N_A$, the slope increases as in Eq. 2.11 to n $(E_D - E_C)/kT$, shown in segment 4.

2.3 Temperature Dependence of the Conductivity: High Concentration ($> 10^{15} cm^{-3}$)

The effects of increased impurity concentration on the carrier concentration and resistivity curves as a function of temperature, are shown in Figs. 12a and b. As N_D increases, $(N_D - N_A)$ increases in the extrinsic region, and the resistivity correspondingly decreases. The

relationship between the resistivity and impurity concentration at low
temperatures becomes more complicated. As the impurity concentration
is increased, a point is reached where charge transport is no longer
due to free carriers, but is instead due to charge transport between
impurities, known as impurity conduction[8]. At medium impurity con-
centrations ($\sim 10^{15} cm^{-3}$), "hopping" transport occurs as electrons hop
from occupied to unoccupied localized donor centers. The resistivity
then follows the exponential relationship, $\rho = \rho_0 \exp(\Delta/T^n)$ for
$0.25 \leq n \leq 1$.[9] The value of n depends upon whether variable range or
nearest-neighbor hopping occurs. At high concentrations ($> 10^{17} cm^{-3}$),
"banding" occurs in which impurity state wavefunctions overlap signifi-
cantly and lose their localized character. This leads to a metallic
type of conduction, with conduction occurring at all temperatures.
Theories concerned with hopping and banding transport in impurity
bands, as well as the effects of compensation will be presented in
Chapter 6.
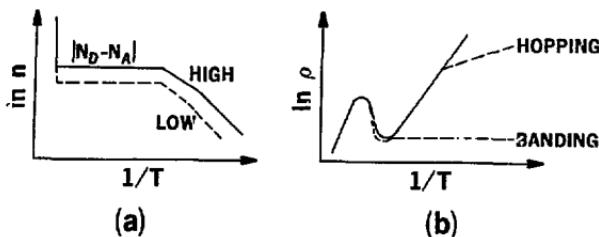
XBL 82B-11224

Fig. 12. Effects on high impurity concentration on (a) carrier concen-
tration and (b) resistivity curves as a function of tempera-
ture.

3. Impurity Doping Methods

3.1 Introduction

Semiconductor doping is accomplished by introducing desired impurities into specified areas of a semiconductor device. Due to the variety of doping requirements needed for modern electronic devices, several doping methods have been developed. Two methods, impurity diffusion and ion implantation, are commonly used to dope standard thin layer devices of thicknesses of about 1000 Å or less. This discussion of doping, however, will emphasize bulk techniques used to dope devices of greater thickness. The two most common bulk doping methods are doping during crystal growth and neutron transmutation doping (NTD).

Because device performance and reliability are critically affected by impurity levels, there is a strong incentive to first develop large, ultra-pure semiconductor single crystals. Once the starting semiconductor material has been purified of foreign atoms, it is then doped deliberately to the desired impurity level. In the case of ultra-pure germanium, a net concentration of shallow impurity centers of about $10^{10} cm^{-3}$, corresponding to a net-impurity concentration of one in more than 10^{12} germanium atoms has been achieved[10].

3.2 Purification

Commercially produced polycrystalline germanium used as starting material normally contains boron, phosphorus and aluminum at levels of ~ 10^{12} to $10^{13} cm^{-3}$. In order to reduce these impurity concentrations by two to three orders of magnitude, one can use the principle of solid-liquid impurity segregation. Thus, for a given impurity there is a specific ratio of concentrations found in the liquid C_L, and in the

solid C_S when the phases are in equilibrium[1] (Fig. 13a). This ratio, called the segregation coefficient, k, is defined as:

$$k = C_S/C_L. \tag{3.1}$$

The value of k in Eq. 3.1 is appropriate only when the interface is at equilibrium. Because the segregation is therefore altered by any finite growth velocity such that impurities must diffuse through a diffusion layer at the interface, an effective segregation coefficient k_{eff} is found to be:

$$k_{eff} = [1+(1/k_0 - 1) \exp(- f\delta/D)]^{-1} \tag{3.2}$$

where D is the diffusivity of impurities in the liquid, f is the growth rate and δ is the width of the diffusion layer.
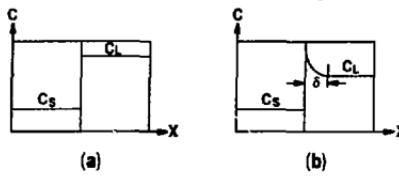
Fig. 13. Solute concentrations at (a) equilibrium and (b) finite growth rate at the solid-liquid interface.

Zone purification and multiple "normal freeze" growth are most commonly used to purify germanium. In zone purification[1], a narrow liquid zone of germanium is melted by means of an RF field which is passed slowly along a long bar of germanium contained in a "boat" (Fig. 14). The molten zone is moved from one end of the bar to the other end, and the process is repeated several times in order to collect the impurities by segregation into one end of the bar.
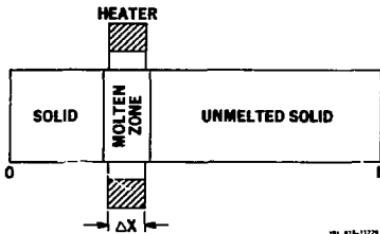
Fig. 14.   Schematic of zone purification process.
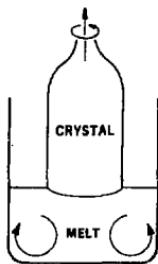
Fig. 15.   Schematic of normal freeze growth method.

In the "normal freeze" method shown in Fig. 15, impurities with
$k < 1$ become concentrated in the melt. This results in a high concen-
tration of impurities in the tail end of the crystal. The pure "seed"
ends of preceding crystals are then used to grow subsequent crystals
of higher purity.

Although both zone purification and the multiple normal freeze
growth method can be theoretically used to produce perfectly pure
crystals, there are practical limitations. Interactions between the
molten germar.ium, the container and the ambient in the zone refiner
or crystal puller limit the purification to concentrations of 10^9 to
$10^{10} cm^{-3}$. In the case of the purest graphite containers available,

phosphorus and boron are found to contaminate germanium[10] to concen-
trations $> 10^{11} cm^{-3}$. Synthetic quartz, a more suitable material, con-
taminates germanium with $\sim 10^{10} cm^{-3}$ phosphorus and higher order com-
pounds of oxygen, aluminum and silicon[10].

In addition, the composition of the atmosphere surrounding the melt
controls the equilibrium between formation and dissociation of impurity
complexes, and the mobility of undesirable impurities. High vacuum is
generally not the preferred ambient because of the very long mean free
paths of atoms and molecules. The long mean free path increases the
probability for an impurity to reach the melted germanium. As a
result, a reducing gas ambient such as hydrogen is usually preferred.

3.3 Doping During Crystal Growth

Doping can also be achieved during single crystal growth. The
most common growth technique for germanium is the Czochralski method .
Doping is achieved either by adding the intended dopant element in
pure form to the melt or by adding a piece of heavily doped semicon-
ductor called the "master dopant" to the melt. The former method is
seldomly used because it is difficult to control accurately the ex-
tremely small amounts of added dopant. Oxidation, evaporation or
interaction with the crucible and atmosphere can reduce the elemental
dopant drastically. Impurity segregation causes a variation of im-
purity concentration along the crystal axis. Impurity striations--
local fluctuations in the impurity concentration--occur in all crystals
grown from the melt. Various methods have been devised to obtain con-
stant impurity concentration profiles. Depending on the segregation
coefficient ($k < 1$), one can add more dopant ($k > 1$) or more pure

semiconductor material (k < 1). These fluctuations are caused by three effects[11]. First, crystal rotation occurs in a non-perfectly cylindrical group of isotherms since the isotherms must be snaped so that a single high-purity crystal of the desired diameter can be grown. For each revolution, the solid/liquid interface may pass through a "hot" or "cold" point, thereby modifying the crystal growth rate and effective segregation coefficient. This results in variations of impurity concentration. Secondly, incorporation of impurities changes the melting point, which can cause oscillations in the growth rate and effective segregation coefficient, as in Fig. 16a and b. The third cause of impurity striations is due to formation of convection cells in the melt. These cells stir the melt in patterns which affect the homogeneity of the impurity concentration. To break these convection cells, one can use magnetic field gradients--which cause eddy currents in the melt--to reduce impurity striations[11]. However, the problem of producing homogeneously-doped and compensated semiconductor single crystals in melt-doped and grown crystals remains[12]. As will be seen later, small doping fluctuations become important at low temperatures. At temperatures below about 1-2 K, dopant concentration fluctuations of a few percent lead to resistivity fluctuations of more than an order of magnitude. As a result, efforts to eliminate this problem have resulted in the development of a doping technique known as neutron transmutation doping (NTD). The NTD process and its advantages will be discussed in the next section.

3.4 Neutron Transmutation Doping

3.4.1 Introduction - As discussed in section 3.3, impurity stria-
tions occur in crystals which have dopants incorporated during growth
from a melt. Because the resistivity of impurity conduction, intro-
duced in section 2.3, is critically dependent on impurity separation
and degree of compensation, it is desirable to dope semiconductors by
a method which allows perfectly homogeneous doping.

Fig. 16. (a) Etched segment of a Te-doped InSb crystal grown in the
presence of (b) thermal oscillations in the melt. (From "J.
Electrochem. Soc." 119, 1218 (1972).

3.4.2 The NTD Process - Neutron transmutation doping[13] is based
upon thermal neutron irradiation of an undoped semiconductor. Because
neutrons are neutral particles, their penetration range is very long.
In the absence of any electrical charge, neutrons readily reach the
nucleus. The number of neutron captures by semiconductor nuclei per
unit volume N is given by:

$$N = N_T \sigma_c \phi \tag{3.3}$$

where N_T is the number of target nuclei per unit volume, σ_c is the
capture cross section, and $\phi = \phi t$ is the fluence (flux times time).

The magnitudes of the impurity concentrations can thus be varied, since they depend on the neutron flux and exposure times. It can be shown that for low neutron energies, the capture cross section is related to the energy by[29]:

$$\sigma_c \ \alpha \ E^{-1/2} \alpha \ 1/v \tag{3.4}$$

where v is the neutron velocity. The cross section is thus related to the probability of interaction between the nucleus and the neutron, such that the probability of neutron capture is increased at low neutron energies.

Since the addition of a neutron causes the nucleus to become excited, the target nucleus emits high energy gamma radiation after neutron capture. The energy of gamma rays can be measured accurately. The gamma ray spectrum is an accurate and unique signature of a given nucleus. Neutron activation analysis[14], a tracer technique which is sensitive to impurity levels as low as $10^9 cm^{-3}$, is based on the measurement of gamma ray spectra. If the product isotope is unstable, further decay occurs until a stable isotopic state is reached.

Before discussing neutron transmutation doping of germanium, we will consider the simpler case of silicon, which is of major technological importance. Of the ~ 8,000 tons of semiconductor silicon produced in 1981, 40 tons were neutron transmutation doped[22,23]. Although this is a small percentage of the total silicon market, NTD Si is critical to the production of very high voltage, high power devices, which are extremely expensive. This is in contrast to the more popular devices of extremely small voltage and low power used in the semiconductor industry.

In the case of silicon, three stable isotopes are present. Absorption of neutrons leads to the following reactions[18]:

$$(92.3\%) \ _{14}^{28}Si(n,\gamma) \ _{14}^{29}Si$$
$$(4.7\%) \ _{14}^{29}Si(n,\gamma) \ _{14}^{30}Si$$
$$(3.1\%) \ _{14}^{30}Si(n,\gamma) \ _{14}^{31}Si \rightarrow \ _{15}^{31}P + \beta^-, \ \sigma_c \ = \ 0.108b$$
$$t_{1/2} \ = \ 2.62h$$
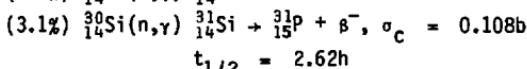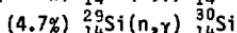
The first two reactions do not produce dopants. However, the ^{30}Si isotope which is 3.1% abundant is transmuted to ^{31}Si which then β^- decays with a half-life of 2.62 h to the stable isotope ^{31}P, a donor. The desired phosphorus isotope further decays:
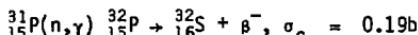
$$_{15}^{31}P(n,\gamma) \ _{15}^{32}P \rightarrow \ _{16}^{32}S + \beta^-, \ \sigma_c \ = \ 0.19b$$
$$t_{1/2} \ = \ 14.3d$$

This process occurs, however, only after substantial dopant levels have been reached.

The undesirable ^{32}P is the primary source of radioactivity in silicon and leads to unwanted sulfur in the crystal. This secondary reaction limits the NTD method to $\rho > 1 \, \Omega cm$ for Si. In the range $\rho < 5 \, \Omega cm$, the ^{32}P activity can be reduced by using low neutron flux densities ($\sim 10 \ n/cm^2 sec$) because ^{32}P production varies with the square of the neutron flux. However, this leads to prolonged irradiation times and unattractively high costs. For higher resistivity material, $\rho > 10 \, \Omega cm$, the formation of ^{32}P can be reduced by using high neutron flux densities ($\sim 10^{15} \ n/cm^2 sec$). Due to the use of shorter irradiation times, there is incomplete decay of the ^{31}Si activity within the radiation time such that there are fewer ^{31}P atoms available for production of ^{32}P.

Although silicon is the only semiconductor which is commercially doped by NTD, the process can be used for other semiconductors. Shown below are the neutron capture reactions which yield dopant isotopes in germanium and gallium arsenide, respectively:

TABLE I.

Isotope Fraction	Reaction	σ_c(b)	$t_{1/2}$	Type
(20.5%)	$^{70}_{32}\text{Ge}(n,\gamma)\ ^{71}_{32}\text{Ge} \rightarrow\ ^{71}_{32}\text{Ga} + K$	3.25	11.2d	p
(36.5%)	$^{74}_{32}\text{Ge}(n,\gamma)\ ^{75}_{32}\text{Ge} \rightarrow\ ^{75}_{33}\text{As} + \beta^-$	0.52	82.8m	n
(7.8%)	$^{76}_{32}\text{Ge}(n,\gamma)\ ^{77}_{32}\text{Ge} \rightarrow\ ^{77}_{33}\text{As} + \beta^- \rightarrow \text{Se} + \beta^-$	0.16	11.3h	n
(60.1%)	$^{69}_{31}\text{Ga}(n,\gamma)\ ^{70}_{31}\text{Ga} \rightarrow\ ^{70}_{32}\text{Ge} + \beta^-$	1.7	21.1m	n
(39.9%)	$^{71}_{31}\text{Ga}(n,\gamma)\ ^{72}_{31}\text{Ga} \rightarrow\ ^{72}_{32}\text{Ge} + \beta^-$	4.6	14.1h	n
(100.0%)	$^{75}_{33}\text{As}(n,\gamma)\ ^{76}_{33}\text{As} \rightarrow\ ^{76}_{34}\text{Se} + \beta^-$	4.4	26.3h	n

Of the above cases of Si, Ge and GaAs, only germanium yields a compensated material, while silicon and gallium arsenide yield strictly n-type dopants. For germanium, the compensation ratio will be:

$$K = \frac{N_D}{N_A} = \frac{[\text{As}] + 2[\text{Se}]}{[\text{Ga}]} = 0.322$$

The values for selenium are counted twice because selenium is a doubly charged donor and can thus compensate two acceptors. We believe that the value K = 0.322 is more accurate than the value K = 0.40 used in other sources, based on older capture cross section data[18,19].

Following neutron irradiation, the NTD material is thermally annealed of radiation damage caused by residual high-energy neutrons present in the thermal neutron beam. The primary sources of radiation damage are the fast neutron knock-on displacements and gamma and beta

recoil damages which produce massive numbers of atom displacements compared to the dopant atoms produced. Typical numbers of displacements for each dopant atom produced are as high as 10^4 to 10^6 in silicon[13]. Of these, the displacements from fast neutron knock-on recoil can be expected to be about 10^3 times higher than the damage from thermal neutron recoil[13]. Fast neutrons therefore dominate the displacement damage unless thermal-to-fast neutron ratios exceed 1000:1. Typically, the ratio of thermal-to-fast neutrons is only about 10:1 to 50:1, but there are reactors which can achieve ratios higher than $1000:1$[20]. The thermal neutron capture cross sections for germanium and gallium arsenide are much larger than those for silicon, as shown in Table I. As a result, the displacement damage by thermal neutrons, relative to fast neutrons, is greater than it is in silicon.

Radiation damage introduces defect levels in the bandgap, which causes reductions in free carrier concentrations, carrier mobility and minority free carrier lifetime. Thermal annealing recovers the electrical activity of the dopant impurities by healing the damage. Although the free carrier concentration and mobility can be recovered during the annealing cycle, the minority free carrier lifetime is not fully recovered. This is not well understood but it is thought that the lifetime is strongly affected by the purity of the starting material and the cleanliness of the reactor[14]. For germanium and silicon, thermal annealing temperatures of 400-450°C and 800-850°C, respectively, are commonly used[21].

3.4.3 The Advantages of the NTD Process — Using the NTD process, one obtains reproducible, homogeneously-doped semiconductors of a known compensation such that NTD is advantageous over conventional doping methods as discussed in section 3.3.

Because all reactors producing NTD material rotate the ingots in order to improve radial uniformity, the accuracy in the doping can be controlled to better than 1% for small samples[14]. This is far superior to conventional methods for which the doping inaccuracy may be as high as 25%[13]. Figure 17 shows the accuracy attainable in terms of percentage deviation of mean dopant concentration. Also shown is a comparison of the spreading resistance as a function of radial distance for both NTD and conventional methods.

The narrow resistivity variation (as low as $\pm$ 4%[13]) attainable in NTD material leads to devices of more uniform electrical characteristics, especially in voltage and switching characteristics. This is particularly important in high power silicon devices, which require high breakdown voltages. The uniform resistivity allows a uniform avalanche breakdown across the device. Finally, the NTD method is particularly desirable for infrared detectors in which considerations of low operating temperatures and high sensitivity often require close compensation of shallow impurities.

% **DEVIATION FROM TARGET**
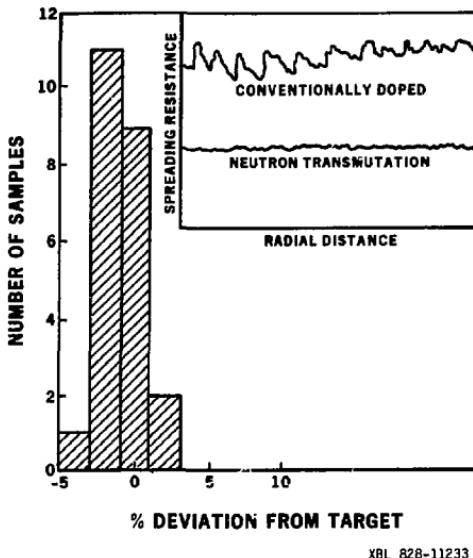
Fig. 17.   Illustration of irradiation target accuracy obtained on sam-
ples irradiated at the University of Missouri Research Reac-
tor.   The insert is a schematic of the spreading resistance
traces across a wafer for conventionally doped and NTD Si.
[After J.M. Meese, Neutron Transmutation Doping in Semicon-
ductors, Plenum Press, New York, 3 (1979)].

4.   Measurement Techniques

4.1   Resistivity Measurements

The resistivity is the inverse of the conductivity $\sigma = ne\mu$, where
n is the concentration of charge carriers (cm^{-3}), e is the charge of
the electron $(= 1.6 \times 10^{19}As)$ and μ is the mobility (cm^2/Vs).   The
resistivity ρ of a homogeneous material is the resistance R of a unit
cube measured between one pair of parallel faces.   With $R = \rho L/A$, we
find $\rho = RA/L (\Omega\ cm)$.   It can be determined by various methods, for
example, by using the so-called "four-point" probe or the "two-point"

probe[24], shown respectively in Fig. 18a and b. With the four-point
probe, one passes a current I through the two outer probes, while the
two inner probes act as high impedance voltage sensors so that the
resistivity ρ is[1]:

$$\rho = (V/I)\pi\delta/\ln2 \ \Omega\,cm \ \text{for} \ \delta << s \tag{4.1a}$$

$$\rho = (V/I)2\pi s \quad \Omega\,cm \ \text{for} \ \delta >> s \tag{4.1b}$$

where δ is the sample thickness and s is the thickness between probes.
Another technique is the two-point probe, used to measure the spreading
resistance of a sample[1,25]. This technique allows the local resist-
ivity on a μm scale to be determined; thus, impurity striations on a
wafer can be measured.

(a)   (b)

XBL 828-11241
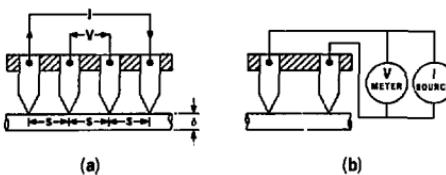
Fig. 18.   (a) The four-point probe. (b) The two-point probe. Probes
           of a hardened and highly conducting alloy are pressed on the
           sample surface.

4.2   Hall Effect

4.2.1 Basic Configuration – The most commonly used method to de-
termine carrier concentration and the type of the carriers (+ or –) is
the Hall effect technique[24]. Together with a resistivity measurement,
the carrier mobility can be determined: $\mu = 1/\rho ne$. The standard Hall
effect configuration is shown in Fig. 19. A current I is passed
through the sample in the x-direction. By applying a magnetic field B
in the z-direction, the Lorentz force acting on electrically charged
carriers causes displacement of the carriers in the y-direction.

There is thus a build-up of an internal electric field (or Hall field) E_H, which will cancel the effect of the Lorentz forces.
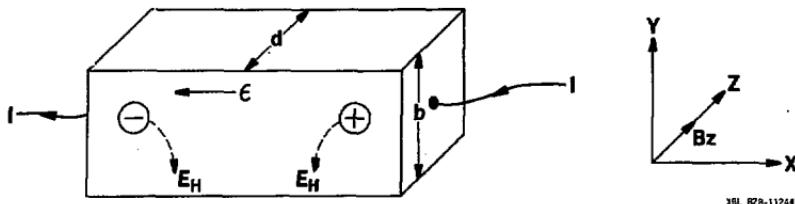
Fig. 19. Basic configuration for Hall effect measurements.

Once equilibrium has been established, in typically less than 10^{-13} sec the Hall force is equal to the Lorentz force, and:

$$e(\vec{v} \times \vec{B}) = e\vec{E}_H$$

$$V_H/b = E_{Hy} = B_z v_x = B_z R_H J_x$$

for a current density $J_x = I/bd$, and Hall coefficient R_H. In the general case, where one type of carrier predominates:

$$J_x = v_x en$$

and $\qquad R_H = 1/ne.$

Above, n is the carrier concentration and e is the charge on an electron. If both electrons and holes contribute to conduction, R_H can be shown to be:

$$R_H = (1/e)[(p - b^2 n)/(p + bn)^2]$$

where $b = \mu_n/\mu_p$ is the ratio of the electron to hole mobility.

    4.2.1 <u>Van der Pauw Method</u> - In 1958, a method of measuring resistivity and Hall effect of flat, thin samples (lamellae) was introduced by L.J. van der Pauw[26]. For this method, the electrical con-

tacts must be sufficiently small and located at the circumference of the sample. Furthermore, the sample should be of constant thickness and must not have isolated holes.

Van der Pauw showed that for an arbitrarily shaped sample of constant thickness δ with successive contacts A,B,C,D as described above and shown in Fig. 20, the resistivity can be expressed as:

$$\rho = (\pi\delta/\ln2)[(R_{AB,CD} + R_{BC,DA})/2] \times f.$$

$R_{AB,CD}$ is the resistance obtained from the voltage across contacts A and B, divided by the current through contacts C and D. $R_{BC,DA}$ is analogous to $R_{AB,CD}$, and f is a function of the ratio $R_{AB,CD}:R_{BC,DA}$ only as shown in Fig. 21[26]. In the case of a circular or rectangular sample, f = 1.
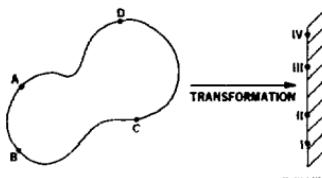

Fig. 20. Van der Pauw's use of conformal transformation to determine the resistivity of an arbitrarily shaped sample of thickness .
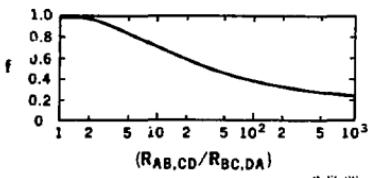

Fig. 21. The function f used to determine the specific resistivity of a specimen with an arbitrary contour as a function of the resistance ratio $R_{12,34}/R_{23,41}$. [after L.J. van der Pauw, Phillips Res. Repts., 13 (1958) 1].

Both the Hall mobility and free carrier concentration can be found by measuring the change of resistance, $R_{BD,AC}$ when a magnetic field B is applied perpendicular to the sample. The hall coefficient R_H is then:

$$R_H = (\delta\Delta R_{BD,AC})/B$$

$\Delta R_{BD,AC}$ is the change of resistance due to the magnetic field. The Hall mobility μ_H is then given by:

$$\mu_H = (\delta\Delta R_{BD,AC})/B\rho$$

and the free carrier concentration is:

$$n = B/e\delta\Delta R_{BD,AC}.$$

Van der Pauw and others have made estimates of the error intro-
duced by using contacts of finite size and not located at the circum-
ference of the sample. It has been shown[25] that the van der Pauw
geometry is quite insensitive to deviations from the ideal geometry.
In Fig. 22, one sees that the error in sheet resistance is only second
order dependent on the ratio of contact length to the length of one
side of a square-shaped sample[27].
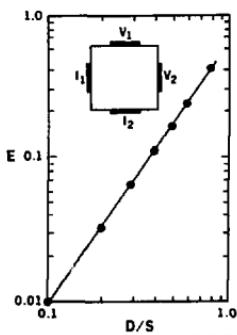
Fig. 22. Normalized sheet resistance error E with contacts centered
on each side of a square specimen with dimensions as shown
in the insert as a function the ratio of contact length to
side of the square. [after M.G. Buehler and J.M. David,
Natl. Bureau of Stds., Special Publ. 400-29 (1967) 64].

5. Experimental and Data

5.1 Sample Preparation*

Wafers of ultra-pure p-type germanium crystal #516 were cut per-
pendicular to the <113> axis of crystal growth (Fig. 23), and were
lapped with 600 and 1900 grit lapping compound. The six wafers, taken
along the lengths 3.3 to 5.2 cm of the 17 cm long crystal, had impur-
ity concentrations of 3.4 x 10^{10} to 4.0 x 10^{10} cm^{-3}. Neutron
transmutation doping (NTD) to gallium concentrations of 2 x $10^{15}cm^{-3}$
$\leq N_A \leq$ 5 x $10^{16}cm^{-3}$ was done on the wafers by J.M. Meese at the
University of Missouri Research Reactor. About one year after
neutron irradiation--after the decay of many half-lives of the longer
living ^{71}Ge ($t_{1/2}$ = 12d)--two samples from each wafer of size
~ 7 x 7 x 2 mm^3 were cut with a string saw and lapped**. This was
followed by etching (~ 15 secs) of the samples in a 3:1 HNO_3:HF so-
lution and quenching in electronic grade methanol. Next, the samples
were thermally annealed at 400°C for six hours in dry argon in order
to heal radiation damage incurred during the NTD process.

In order to compare NTD germanium (with compensation K = 0.322)
with nearly uncompensated germanium, wafers of ultra-pure crystal #582
were cut at lengths 13.2, 14.5 and 15.5 along the crystal as shown in
Fig. 24. These wafers have gallium concentrations of 2.4 x $10^{15}cm^3$

---

*Details of sample preparation are described in the Appendix.
**Additional samples of size ~ 0.4 x 0.4 x 0.6 mm^3 were later tested
with resistance as a function of T, identical to that of the larger
samples.
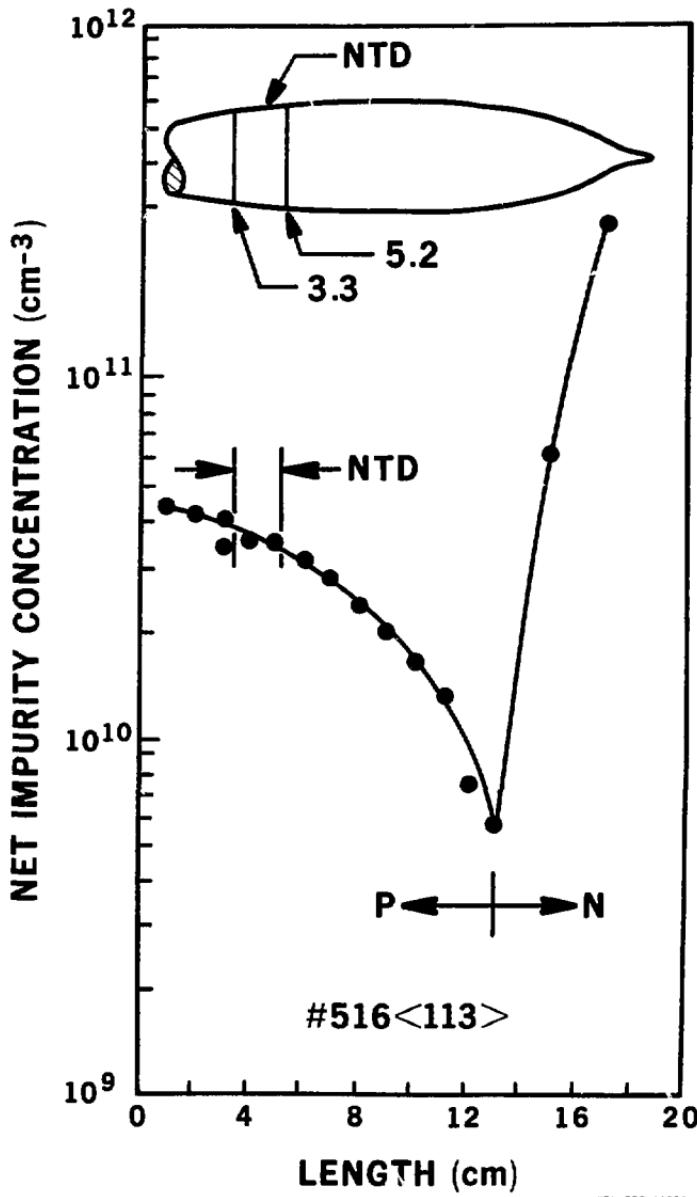
Fig. 23. Impurity profile of crystal selected for NTD.
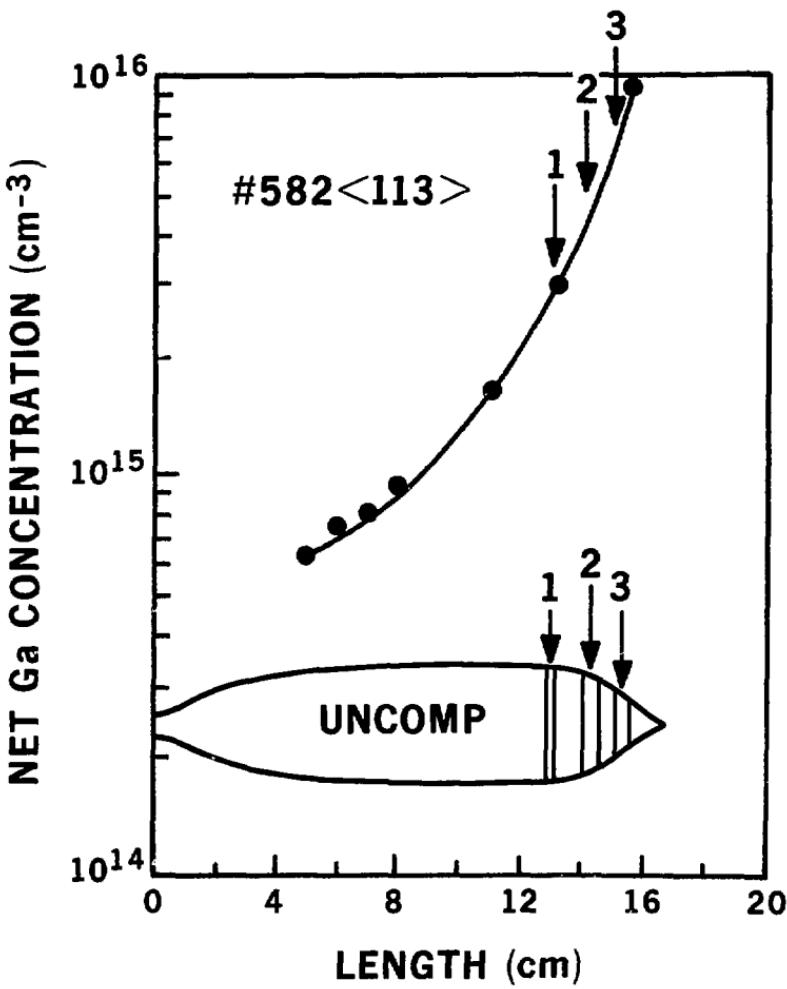
Fig. 24. Impurity profile of melt-doped crystal.

to $1.1 \times 10^{16} \text{cm}^{-3}$, respectively, as shown in the impurity concentration profile. Two samples of size ~ 7 x 7 x 2 mm^3 were cut from each wafer.

5.2 Contact Preparation

In order to provide ohmic p^+ contacts over a large temperature range, the samples were doubly implanted at room temperature with boron ions at 100 keV at a dose of $2 \times 10^{14} \text{cm}^{-2}$ and 130 keV at a dose of $4 \times 10^{14} \text{cm}^{-2}$. This was followed by annealing at 250°C for one hour in dry argon. The top 500 Å of the germanium surface were etched off in a 5% NaOCl solution for 30 seconds. RF sputtering of 400 Å of titanium and 8000 Å of gold in argon was followed by annealing for 20 minutes at 250°C in argon. To obtain contacts in the corners of the ~amples on both sides, one protects the small corner contact area with Picein wax and etches the gold in a 1:4 I_2 + KI solution. The titanium layer stops this etchant and protects the underlying boron implanted layer. The titanium was removed in a few seconds in 1% HF. Finally, the p^+ layer was removed in a 3:1 HF:HNO$_3$ etching solution. After removal of the Picein wax from the corner contact areas, 5 mil copper wires were soldered onto the contact pads using pure, fresh indium without any application of flux. Finally, pure indium foil strips were used to connect the front and back side contacts in each corner as in Fig. 25. Charge injection from each double pad is approximating the behavior of the ideal contact geometry very well. Ideal contacts would have been infinitely narrow, positioned along the edge of each corner.
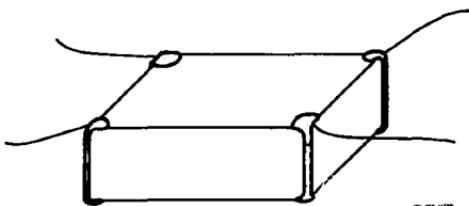
Fig. 25. Method of forming electrical contacts on germanium sample.

5.3 Measurement

Variable temperature Hall effect measurements (van der Pauw method)
were made on the p—type Ge samples over the temperature range 0.3 K to
300 K using liquid helium[28]. A magnetic field of 6000 gauss was
used in the temperature range 300 K — 77 K, while a field of 1200 gauss
was applied below 77 K. Thus, magnetoresistance effects were mini-
mized. The Hall effect apparatus[29] shown in Fig. 26 uses a silicon
diode thermometer screwed down to a copper base which can be used over
a temperature range of ~ 1.5 K to 300 K. The samples, positioned along
the extended copper base shown in Fig. 27, lie in an evacuated chamber
(~ 10^{-6}torr), and are surrounded by three radiation shields to pre-
vent penetration of light or thermal energy. Cigarette paper lined
with high vacuum grease lies between the cold finger and the sample
to prevent electrical contact and subsequent short circuit of the Ge
sample. Helium is passed from a dewar through the evacuation shroud
into the sample chamber. For measurements down to 1.5 K, the liquid
^{4}He bath is pumped on with a rough pump down to below 1 mm.

5.4 Data

Plots of resistivity and concentration as a function of inverse
temperature are shown, respectively, in Figs. 28 and 29. From the

FLEX LINE

HELIUM CYLINDER

PRESSURE
REGULATOR

VACUUM SHROUD

SUITABLE SHROUD
SUPPORT & CLAMP

LIQUID HELIUM
DEWAR
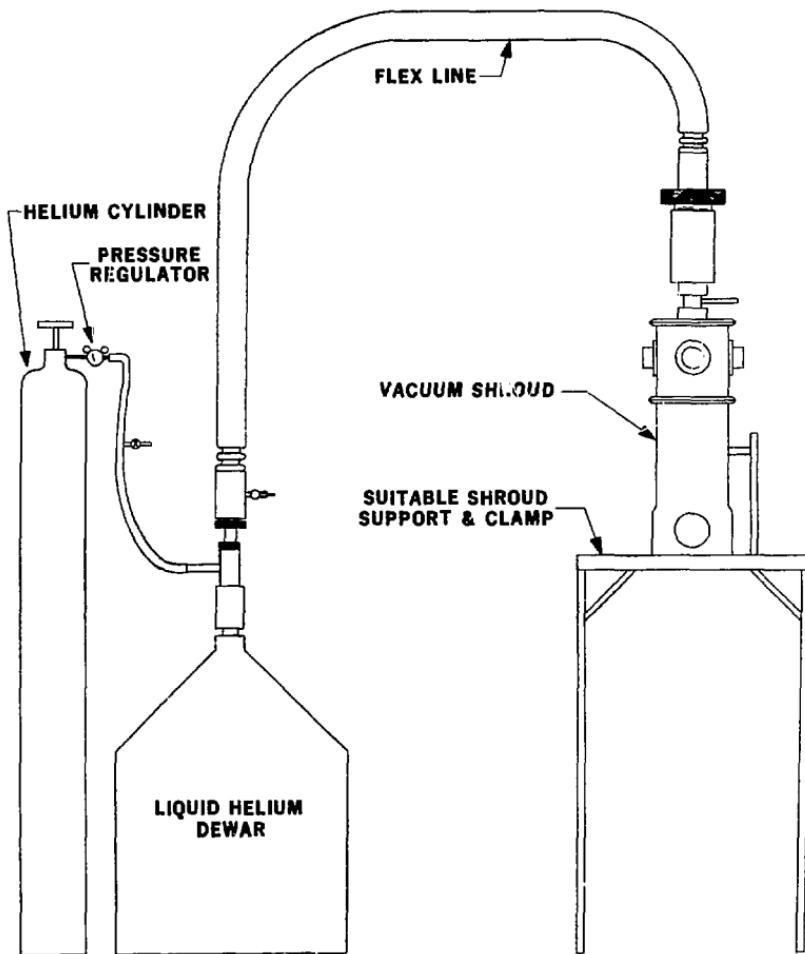
XBL 828-11237

Fig. 26. Variable temperature Hall effect apparatus.

¾"I.D. S/S
72" FLEX HOSE

ADJUSTABLE THERMAL
IMPEDANCE & PHASE
SEPARATOR

EVACUATION
VALVE

SAFETY PRESSURE
RELIEF

FLOW VALVE
REGULATOR

ADJUSTABLE POSITION
PRESSURE HAT

PRESSURE RELIEF
VENT VALVE

HELIUM VENT—VACUUM
PUMPING LINE FOR
OPERATION BELOW 4.2K

PRESSURE RELIEF

ELECTRICAL
FEEDTHROUGH FOR
INSTRUMENTATION
& HEATER LEADS

HIGHLY POLISHED
ALUMINUM RADIATION
SHIELD

LIQUID HELIUM
WITHDRAWAL
TUBE—INSERTED
IN DEWAR

VACUUM SHROUD

COOPER SAMPLE MOUNT
WITH 50 OHM WOUND
HEATER & PROVISION
FOR DT—500 SENSOR

SAMPLE POSITION
(TYPICAL)

OPTICAL PORTS

XBL 828-11242

Fig. 27. Schematic of sample chamber.
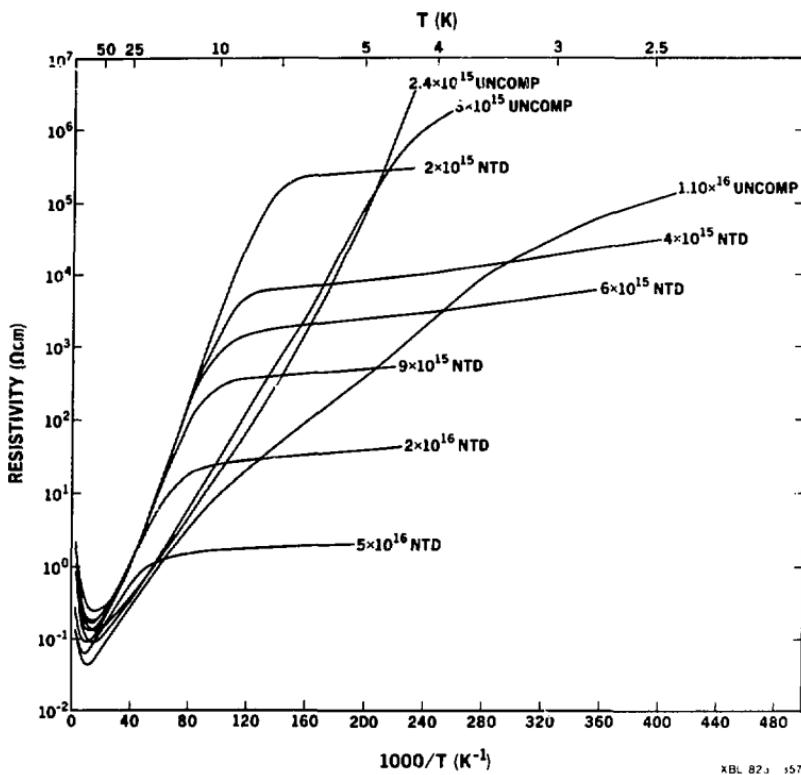
Fig. 28. Plots of resistivity versus 1000/T for NTD Ge and uncompensated Ge samples.
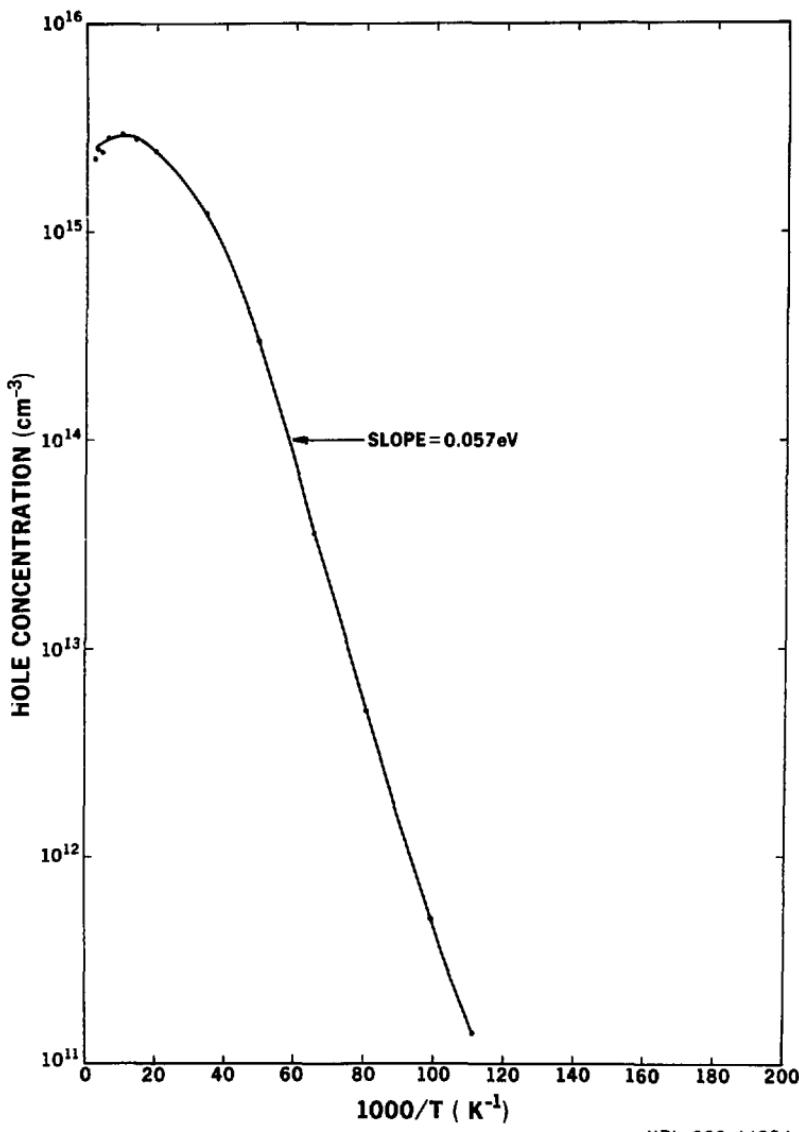
Fig. 29. Hole concentration versus inverse temperature.

resistivity plots, values of Δ and ρ_0 which satisfy the relation $\rho = \rho_0 \exp(\Delta/T^n)$ have been derived for the low temperature range and have been tabulated in Table II for the NTD Ge samples.

TABLE II.

| Sample	$N_A - N_D$ (cm^{-3})	ρ_0 $(\Omega\ cm)$	Δ (K)
NTD 1	2.0×10^{15}	1.4×10^5	8.95
NTD 2	4.0×10^{15}	4000.0	6.90
NTD 3	6.0×10^{15}	1230.0	6.72
NTD 4	9.0×10^{15}	430.0	4.90
NTD 5	2.0×10^{16}	34.0	4.39
NTD 6	5.0×10^{16}	3.3	2.82
UNCOMP 1	2.4×10^{15}		
UNCOMP 2	3.0×10^{15}		
UNCOMP 3	1.1×10^{16}		

Plots of $\ln \rho$ versus T^{-n} for n equal to 1, 1/2 and 1/3 have been made in order to determine the best fit for the value of n. These plots are shown for samples NTD Ge 4 and NTD Ge 5 in Figs. 30 and 31, respectively. As can be seen, the closest fit is obtained with $n = 1/2$; however, the quality of the fit does not depend critically on the value of n. In Fig. 29, the slope of the hole concentration versus $10^3/T$ is shown to approximately satisfy the relationship $n \propto \exp[(E_V - E_A)/2kT]$, as described in section 2.2. The majority impurity, gallium, is located 0.0108 eV above the valence band. This corresponds to a slope of 0.054 eV for uncompensated material. Our data shows a slope of 0.057 eV down to $p \sim 10^{12} cm^{-3}$ in very good agreement with theory.
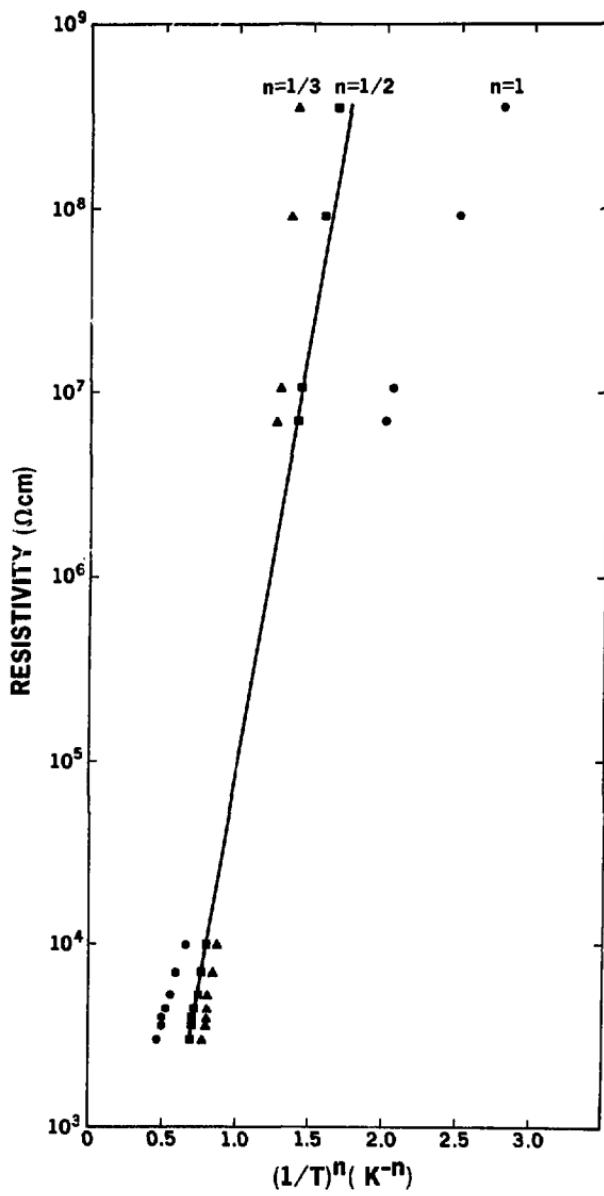
Fig. 30. Resistivity versus $(1/T)^n$.

XBL 828-11256
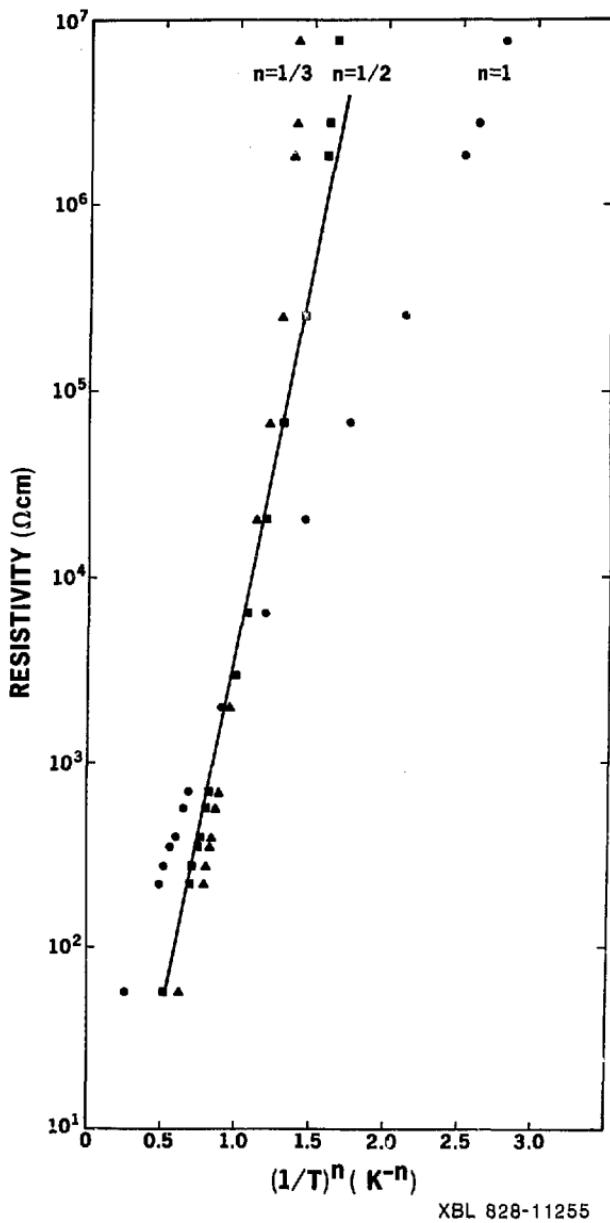
Fig. 31. Resistivity versus $(1/T)^n$.

XBL 828-11255

6. Theories for Electrical Conduction in Semiconductors

In the following discussion, models incorporating the movement of electrons in n-type material will be used, although our experimental results have been obtained with p-type Ge. This has been done in an effort to describe the conduction processes in a simple manner, by avoiding the complications which arise in considering the differences between holes and electrons. This has also been done in view of the fact that no theories have been developed specifically for the conduction mechanisms in heavily-doped and compensated p-type semiconductors.

6.1 Low Temperature Impurity Conduction Mechanisms

Impurity conduction, introduced in section 2.3, was first observed by Busch and Labhart[30] in SiC and later by Hung and Gleissman[8] in Ge. Impurity conduction, unlike ordinary semiconduction, increases nearly exponentially with impurity concentration. This led Hung[8] to suggest that, at temperatures below about 5 K in Ge, impurity conduction occurs because of charge exchanges between impurity sites. For impurity centers which have a small overlap of their wavefunctions, this exchange occurs due to the probability that a carrier can tunnel from an occupied to an unoccupied impurity center.

This can occur only if there is some compensation in order to provide unoccupied sites. For low impurity concentrations, the effect of adding compensators is to lower the resistivity ρ of impurity conduction since there is the creation of more empty centers into which carriers can jump, shown in Fig. 32a. At higher degrees of compensation, ρ increases due to the decreasing number of mobile carriers occupying

majority centers (Fig. 32b). Finally, in the case of complete compensation, impurity conduction vanishes. Then, as in Fig. 32c, all donors are empty and all acceptors are occupied with electrons. Since the overlap is small, impurity conduction is noticeable only at low temperatures when the number of carriers excited into the conduction band is extremely small.
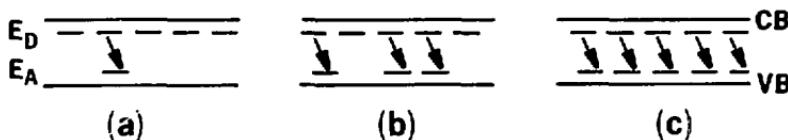
Fig. 32. The effects of (a) low compensation, (b) higher compensation and (c) complete compensation for low impurity concentrations ($<10^{15}$cm^{-3}).

As the concentration of impurities increases, the overlap of the wavefunctions of adjacent impurities becomes so strong that carriers are no longer localized around individual impurities and conduction can proceed without compensation. The resistivity is then expected to be finite for zero compensation, and to increase steadily until it becomes infinite for complete compensation. A metallic type of conduction then occurs. Here, metallic refers to those materials whose conductivity approaches a finite value at absolute zero temperature. "Insulating" materials then, are materials which approach zero conductivity at absolute zero temperature.

Mott introduced the idea[4] that this transition from tunnelling to metallic type of conduction may occur abruptly at a critical concentration n_c given by:

$$n_c^{1/3} a_H^* = 0.26 \tag{6.1}$$

where a_H^* is the effective Bohr radius of the impurity center as in Eq. 1.22. For germanium, $n_c \simeq 1.7 \times 10^{17} \text{cm}^{-3}$ and for silicon, $n_c \simeq 1.9 \times 10^{18} \text{cm}^{-3}$. The value of the conductivity when metallic conduction occurs was then shown to be:

$$\sigma_c = 0.026 \ e^2/hd_c \tag{6.2}$$

where d_c, the average distance between impurity centers at n_c, is about 2.5 a_H^*. The result for the conductivity in Eq. 6.2 corresponds to the value of the conductivity which would be obtained in Eq. 1.33, for values of $(V_c/B)_{crit} = 2$ and number of nearest neighbors, $z = 6$. That $z = 6$ is used is based upon the assumption of a random distribution of centers. Equations 6.1 and 6.2 apply to impurity concentrations just above those of the experimental results. For our data which lies in the transition region ($\sim 10^{15} \text{cm}^{-3}$ to 10^{16}cm^{-3}), an explanation of impurity conduction is given in section 6.2.

6.2 Characteristic Concentration Regions

Conduction processes in a doped semiconductor generally depend on three parameters: temperature, impurity concentration and compensation K. There are three regimes of impurity conduction in the metal-insulator transition. In the low concentration regime, for which $d_c > 5a_H^*$ (corresponding to $|N_A - N_D| < 10^{16} \text{cm}^{-3}$ for Ge), conduction occurs in the conduction band[9] via electrons excited from the D° donors with an activation energy ε_1, as in Fig. 33, curve A. This is also shown experimentally in Fig. 28 in the curves of ρ versus $10^3/T$ in the range 100 K < T < 10 K. At low temperatures, conduction occurs by phonon-assisted hopping from occupied to unoccupied impurity centers with an activation energy ε_3.
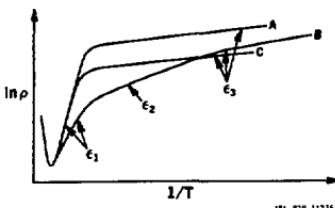
Fig. 33. Activation energies ϵ_1, ϵ_2, ϵ_3 for the three regimes of impurity conduction in the metal-insulator transition.

The intermediate concentration regime, with $5 \geq d/a_H^* > 3$, corresponds to $10^{16} cm^{-3} \leq N_A - N_D \leq 6 \times 10^{16} cm^{-3}$. In this regime, there are three different energy bands which dominate in the three temperature regions of Fig. 33, curve B. As before, there is an activation energy ϵ_1 for conduction to occur in the conduction band at high temperatures. In the intermediate temperature region (#15 K < T < 4 K), conduction occurs with an activation energy, ϵ_2, via doubly occupied donors in the D^- band. The D^- states correspond to donors which are negatively charged by binding an extra electron. The binding energy is $\epsilon_D \simeq 0.01 \epsilon_o$, where ϵ_o is that binding energy for an isolated hydrogen-like donor. Thus, their energy is larger than that of the D° states, but less than that of the conduction band electrons. The bands for the D° and D^- states are known as the lower and upper Hubbard bands, respectively. The D^- states are only important for conduction in a limited concentration region before they merge with the ground states and form metallic conduction at high impurity concentrations. This activation energy, ϵ_2 of the D^- states, is noticeable in Fig. 28, for the uncompensated germanium sample of $1.1 \times 10^{16} cm^{-3}$ impurity concentration. Finally, at low temperatures, hopping conduction occurs with an activation energy ϵ_3.

The metallic impurity band range begins at the edge of the metal-insulator transition, at the critical concentration n_c of Eq. 6.1. The corresponding resistivity as a function of temperature is shown in curve C of Fig. 33. Values of the activation energies ϵ_1, ϵ_2 and ϵ_3 are tabulated in Table III. A plot of activation energy versus carrier concentration is shown in Fig. 34.

TABLE III.

Sample	$N_A - N_D$ (cm^{-3})	ϵ_1 (eV)	ϵ_2 (eV)	ϵ_3 (eV)
NTD 1	2.0×10^{15}	1.19×10^{-2}	--	7.72×10^{-4}
NTD 2	4.0×10^{15}	1.14×10^{-2}	--	5.95×10^{-4}
NTD 3	6.0×10^{15}	1.12×10^{-2}	--	5.79×10^{-4}
NTD 4	9.0×10^{15}	9.91×10^{-3}	--	4.22×10^{-4}
NTD 5	2.0×10^{16}	7.89×10^{-3}	--	3.78×10^{-4}
NTD 6	5.0×10^{16}	5.63×10^{-3}	--	2.43×10^{-4}
UNCOMP 1	2.4×10^{15}	8.64×10^{-3}	--	Undetermined
UNCOMP 2	3.0×10^{15}	7.06×10^{-3}	--	Undetermined
UNCOMP 3	1.1×10^{16}	5.47×10^{-3}	3.04×10^{-3}	1.31×10^{-3}

6.3 Density of States for the Metal-Insulator Transition

Density of states diagrams for the concentration regimes of section 6.2 are shown[9] in Fig. 35. In Fig. 35, n increases by a factor of about 50 from (a) to (d), so that the scale of N(E) increases proportionally. In Fig. 35a, for $n \ll n_c$, the neutral donor states $D^\bullet$ lie ϵ_D below the conduction band edge, while the singlet D^- states are barely bound at the band edge. Because their wave functions are about four times broader than those of the $D^\bullet$ states, they form a
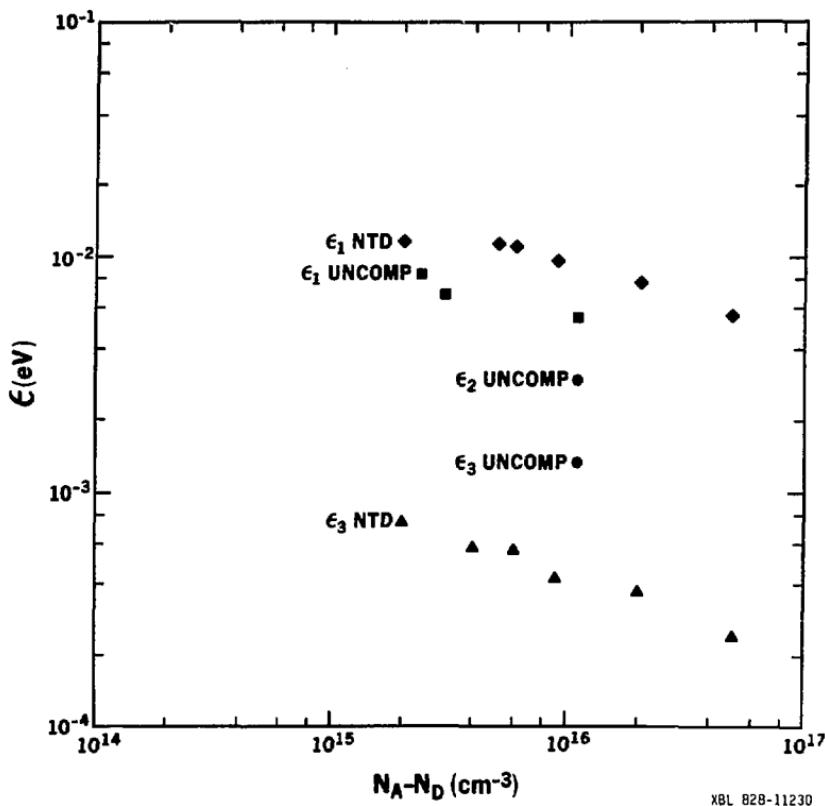
Fig. 34. Activation energies, ϵ_1, ϵ_2 and ϵ_3, versus carrier concentration, $N_A - N_D$, for both NTD Ge and uncompensated Ge samples.

wider band. The Anderson localization criterion, described in section 1.9, will then no longer hold for the upper Hubbard band. If E_c is defined as the mobility edge of the D^- band, the energy into this band is $(E_c - E_F)$.
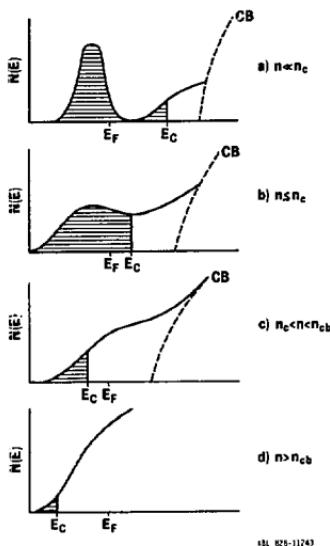
Fig. 35. Density of states N(E) as a function of increasing net impurity concentration n.

As the impurity concentration increases to $n < n_c$ (in Fig. 35b), the D^o and D^- bands merge due to stronger overlap of wavefunctions and ϵ_2 decreases. At $n = n_c$, $E_c = E_F$ and $\epsilon_2 = 0$ because the states near the Fermi level become extended, and the transition to the metallic impurity band conduction occurs. As n increases to $n > n_c$, the conduction band edge shifts downward due to the screening effect of

the positively charged donor ions (as in section 1.6.1), which causes the dielectric constant to increase (Fig. 35c).

There is another transition which occurs at a concentration n_{cb}, in which the conduction band edge falls below the Fermi level, and very few states are localized (Fig. 35d). Thus, for $n \geq n_{cb}$, truly metallic conduction as is found in an impure material prevails.

6.4 Effects of Compensation

In applying the ideas of sections 6.1 to 6.3, the Fermi level E_F cannot always be calculated by integrating the product of $N(E)F(E)$ in Eq. 1.18 and applying charge neutrality as described in section 1.4. This is because the sum of the concentrations $[D^\circ] + [D^+] + [D^-] = [D]$ must be maintained, and because the relative density of states changes with compensation and carrier excitation. For example, compensation increases $[D^+]$ and decreases $[D^-]$, consequently raising E_c and decreasing E_F. This increases $\varepsilon_2 = (E_c - E_F)$ to the point that conduction in the D^- band can no longer compete with ε_3 activated hopping in the $D^\circ - D^+$ band, and we no longer see conduction in the upper Hubbard band at high compensation. Compensation also decreases the metal-insulator transition because the positively-charged donor sites (in n-type material) which are randomly distributed in the material, add to the variation in electric fields which act upon the remaining donor sites. This produces Anderson localization, as described in section 1.9.

6.5 Theories of the Metal-to-Insulator Transition

Theories of the metal-to-insulator transition for doped semiconductors are concerned with impurity conduction in the form of thermally-activated hopping as described in section 6.2. Two types of

hopping can be distinguished: "nearest-neighbor" hopping and "variable range" hopping.

"Nearest-neighbor" or "Miller-Abrahams" hopping[31] uses as a basis the value of the overlap energy integral I given in Eq. 1.32c. It is then assumed that for hydrogen-like functions, the value of I may be written as:

$$I = \frac{3}{2}(1 + \alpha d_c) + \frac{1}{6}(\alpha d_c)^2 \quad e^2\alpha/k \quad \exp(-\alpha d_c) \tag{6.3}$$

where d_c is the distance between impurity centers and $\alpha = 1/a_H$. In the theory of Miller and Abrahams, the exponential term of Eq. 6.3 is taken to be small, such that an electron moves only to its nearest neighbor and the resistivity will be:

$$\rho = \rho_0 \exp(\epsilon_3/kT). \tag{6.4}$$

In the above expression, the activation energy, ϵ_3 is given by:

$$\epsilon_3 = (e^2/\kappa)(4\pi N_D/3)^{1/3}(1 - 1.35 K^{1/3})$$

for compensation $K = N_A/N_D$ and $K < 0.03$. For higher K, a more complicated expression is obtained in which ϵ_3 reaches a minimum near $K = 0.5$. Their theory is found to be in good agreement only for low impurity concentrations ($< 10^{15} cm^{-3}$) in both germanium and silicon.

"Variable-range" hopping introduced by Mott[32] gives a resistivity relationship of the form:

$$\rho = A \exp(B/T^{1/4}) \tag{6.5}$$

where A and B are experimentally determined constants. In this one-dimensional derivation, Mott considers that in the low temperature limit, the probability of finding a phonon of energy large enough to

initiate hopping between neighboring states of differing energies
becomes very small. As a result, the electron hops large distances to
find a state of similar energy. In this theory, charge transport is
due to the motion of electrons near the Fermi level. An electron is
found to hop to a site of energy $E = E_F + W$ at a distance R from the
initial site, when the hopping rate ρ is at a maximum:

$$\rho \; \alpha \; \exp(-2\alpha R - W/kT). \tag{6.6}$$

The optimum values of R and W are found by assuming a density of states
of the form[57]:

$$N(E) = N_0 E^\gamma \tag{6.7}$$

where N_0 and γ are postive constants and E is the energy difference
from the Fermi level. The number of sites within a radius R and energy
W available to an electron near the Fermi level is:

$$(4\pi R^3/3) \; \int_0^W N(E)dE. \tag{6.8}$$

If Eq. 6.8 is set equal to one, the distance R that an electron must
hop to find at least one unoccupied state of energy $E \leq E_F + W$ is:

$$R = [3(\gamma + 1)/4\pi N_0 W^{(\gamma + 1)}]^{1/3} \tag{6.9}$$

By substituting Eq. 6.9 into Eq. 6.6, the optimum hopping energy is
obtained:

$$W = [(\gamma + 1)^4 (2\alpha kT)^3/36\pi N_0)]^{1/(\gamma + 1)} \tag{6.10}$$

Thus, the hopping rate and resistivity are related to the temperature:

$$\ln \rho = T^{(\gamma+1)/(\gamma+4)} \tag{6.11}$$

Setting $\gamma = 0$, Mott's expression (Eq. 6.5) for variable range hopping
is obtained. However, expressions 6.5 through 6.11 neglect intersite
electron-electron interactions. Specifically, in the low temperature

limit, intersite Coulomb interactions introduce a gap at the Fermi level for one-electron hops, so that $N(E_F)$ vanishes at E_F and is finite elsewhere.

According to Mott, the Coulomb gap of one-electron hops disappears as variable range hopping sets in[4]. He predicts that even in the limit as $T \to 0$, Eq. 6.5 is still valid, if one uses a smaller, temperature-dependent value of A. Efros[34], on the other hand, believes that a residual gap remains, even for multi-electron hops. In Efros' theory, the density of states with energy near the Fermi level for polaran-like excitations approaches zero as:

$$N(E - E_F) = 3\kappa^3(E - E_F)^2/2\pi e^6.$$

Efros then concludes that the low temperature resistivity should be of the form:

$$\rho \propto \exp(T_0/T)^{1/2}$$

where $T_0 = e^2/k\kappa a^*$. Only the theory of Efros is consistent with the data for the NTD samples, as shown in Figs. 30 and 31 of ρ versus T^{-n} for NTD Ge 4 and NTD Ge 5 at $T < 5$ K. This temperature dependence has also been observed in both bulk GaAs[35] and n-Si[36]. Using a value of $a^* = 45$ for Ge, one obtains $T_0^{1/2} = 8.6$ $K^{1/2}$ which is in fair agreement with the experimental values of Table 1 for the NTD Ge samples. However, Efros' theory neglects an explicit explanation of dopant concentration and compensation dependence for the value $T_0^{1/2}$. In reviewing the theories of the metal-to-insulator transition for doped semiconductors, it is apparent that the dependence of the critical concentration n_c on compensation is not accounted for. As compensation increases,

the effects of disorder and Anderson localization become dominant so
that compensation clearly needs to be included in the model of hopping
conduction. However, the role of electron-impurity interactions are
not well understood, and the various theories of hopping continue to
be controversial. As a result, additional low temperature measure-
ments and further studies of the effects of compensation are needed.

7. Conclusions

The resistivity of neutron transmutation doped germanium (NTD Ge)
has been measured as a function of net-impurity concentration
$(2 \times 10^{15} cm^{-3} \leq N_A - N_D \leq 5 \times 10^{16} cm^{-3})$, and temperature
$(0.3 K \leq T \leq 300 K)$, at a compensation $K = 0.322$. The NTD Ge samples
were compared with ultra-pure gallium-doped samples, which are nearly
uncompensated $(2.4 \times 10^{15} cm^{-3} \leq [Ga] \leq 1.1 \times 10^{16} cm^{-3})$.

Our results indicate that the resistivity can be approximated by
$\rho = k_1 \exp(\Delta/T^{1/2})$ in the hopping conduction regime down to 0.3 K.
This resistivity dependence on temperature is most consistent with
Efros' theory for variable range hopping, where Efros predicts that
$\ln \rho \propto (T_0/T)^{1/2}$ with $T_0 = 74.0 K^{1/2}$ for germanium. However,
Efros' theory does not include an explicit explanation of dopant con-
centration and compensation dependence for the value $T_0^{1/2}$. In
the NTD Ge samples, for a given $N_A - N_D$, we find that k and Δ are
constant within the crystals down to dimensions of ~ 0.3 mm and most
probably much smaller, and they can be reproduced in any high-purity
Ge single crystal by a predictable thermal neutron exposure and a

thermal annealing cycle. Neutron transmutation doping is thus advan-
tageous over conventional doping of a crystal during the melt because
it allows reproducible homogeneous doping at a fixed, known compensa-
tion. This makes NTD Ge a prime candidate for very low temperature
bolometer applications.

APPENDIX: SAMPLE PREPARATION

A. Wafer Preparation

1. Obtain ultra-pure germanium crystal wafers which have been neutron transmutation doped to the desired impurity levels.

2. About one year after neutron irradiation, after many half-lives of the longer living ^{71}Ge ($t_{1/2} = 12$ days), the wafers are annealed in dry argon gas to heal the radiation damage, according to the schedule below:

XBL 828-11231
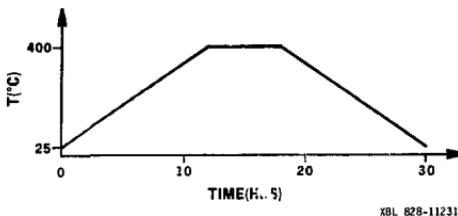
By slowly cooling the wafers, unwanted impurities such as copper are forced to precipitate out of the wafers.

3. Mount wafers onto a carbon block, using dental wax as the adhesive.

4. Cut the wafers to the desired size using a wire saw. (Our samples were cut, using a 0.010" thick wire saw, to sizes of ~ 7 x 7 x 1.9 mm^3). The samples are simultaneously cut and lapped by using a suspension of 1900-grit lapping compound in mineral oil as an abrasive.

5. Remove the samples from the carbon block.

6. Cleanse the samples of the remaining dental wax using pure tri-chloroethylene (TCE) which is heated to below its boiling point.

7. Dry the samples in air.

8. The samples are etched in a 3:1 HNO_3:HF solution for about 45 secs ~ 1 min., or until a shiny, damage-free surface appears.

9. Quench the wafers in methanol.

10. Soak the wafers in 1% HF for ~ 10 min. or until the wafers are hydrophobic.

11. Quickly dry the samples in air.

B. Ion Implantation

1. The samples are doubly ion implanted on both sides at room
   temperature with boron ions at an energy of:

   $\qquad$ 100 keV at a dose of $2 \times 10^{14} cm^{-2}$
   and $\qquad$ 130 keV at a dose of $4 \times 10^{14} cm^{-2}$

2. The top 500 Å of Ge is etched off in a 5% NaOCl solution for ~ 30
   sec in order to reach the depth of near maximum B concentration.

3. Anneal the samples at 250°C for one hour in dry argon.

C. Metallization

1. RF sputtering is used to deposit 400 Å of Ti, followed by 8000 Å
   of Au on the sample surfaces on both sides.

2. Samples are etched briefly (~ 10 sec) in 3:1 HNO_3:HF to remove
   surface contamination.

3. Quench the samples in methanol and dry them in air.

4. Samples are annealed at 250°C for one hour in dry argon.

5. The sample corners on the front and backsides are protected with
   Picein wax (S-14975, low T; Sargent Welch). The Picein wax is
   diluted with TCE to the desired consistency, painted onto the
   corners, and allowed to dry.

6. The bare sides of the samples are lapped gently with 1900-grit
   lapping compound to remove any Au and Ti deposited on them.

7. The Au, not protected by Picein wax, is removed from the top and
   bottom surfaces in a 4:1 $KI:I_2$ solution.

8. Similarly, the excess Ti is instantly etched away in a 1% HF
   solution.

9. The samples are etched for ~ 20 sec in a 3:1 HNO_3:HF solution,
   in order to remove the boron implanted layer from the non-contact
   areas.

10. Quench the samples in methanol.

11. Transfer the samples to pure TCE, and remove the Picein wax.

12. Quench and rinse the samples in methanol.

13. Dry the samples rapidly in air.

D. Electrical Contact Formation

1. Using a soldering iron, melt a very small amount of In onto the four Au contacts on the front side of the sample.

2. Cut and tin 5 mil Cu-40 wire lengths with Sn-60 solder flux.

3. Melt a very small amount of In onto one end of the tinned wire lengths.

4. Attach one tinned and In-coated wire end to each of the sample corners on the front side, by re-heating the corners just long enough to re-melt the In.

REFERENCES

1. L. Solymar and D. Walsh, Lectures on the Properties of Materials, 2nd ed., Oxford University Press (1979).

2. C. Kittel, Introduction to Solid State Physics, 5th ed., John Wiley and Sons, New York (1976).

3. B. Hannay, Semiconductors, Reinhold Publishing Co. (1959).

4. N.F. Mott, Metal-Insulator Transitions, Barnes and Noble Books, New York (1974).

5. M.A. Omar, Elementary Solid State Physics: Principles and Applications, Addison-Wesley Publishing Co. (1975).

6. W. Kohn, Solid State Physics, F. Seltz and D. Turnball, eds., Academic Press, Inc., New York (1957).

7. D.J. Thouless, "The Anderson Model for Disordered Solids," L.R. Friedman and D.P. Tunstall, eds., Scottish Universities Summer School in Physics, St. Andrews, Scotland (1978).

8. C.S. Hung and J.R. Gleissman, "Phys. Rev.," 79, 726 (1950).

9. H. Fritzsche, "The Metal Non-Metal Transition in Disordered Systems," L.R. Friedman and D.P. Tunstall, eds., Scottish Universities Summer School in Physics, St. Andrews, Scotland (1978).

10. E.E. Haller, W.L. Hansen and F.S. Goulding, "Adv. Phys.," 30, No. 1, 93 (1981).

11. W. Keller and A. Muhlbauer, Floating-Zone Silicon, Marcel Dekker, Inc. (1981).

12. R.G. Rhodes, Imperfections and Active Centers in Semiconductors, The MacMillan Co., New York (1964).

13. J.M. Meese, ed., Neutron Transmutation Doping in Semiconductors, Plenum Press, New York (1979).

14. J.M. Meese, D.L. Cowan and M. Chandrasekhar, "IEEE Trans Nucl. Sci.," NS-26, No. 6, 4858 (1979).

15. D.E. Cullen and P.J. Hlavac, ENDF/B Cross Sections, Brookhaven National Laboratory, Upton, New York (1972).

16. M. Tanenbaum and A.D. Mills, "J. Electrochem. Soc.," 108, 171 (1961).

17. C.M. Lederer and V.S. Shirley, eds., Table of Isotopes, 7th ed., John Wiley and Sons, New York (1978).

18. C.M. Lederer, J.M. Hollander and I. Perlman, eds., Table of Isotopes, 6th ed., John Wiley and Sons, New York (1967).

19. H.C. Schweinler, "J. Appl. Phys.," 30, 1125 (1959).

20. T.G.G. Smith and A.E. Harwell, "Neutron Doping of Silicon in the Harwell Research Reactors," J.M. Meese, ed., Plenum Press, New York (1979).

21. H. Fritzsche and M. Cuevas, "Phys. Rev.," 119, No. 4, 1238 (1960).

22. T.G.G. Smith, "Future Reactor Capacity for the Irradiation of Silicon for the Purpose of Neutron Transmutation Doping," Proceedings of the Fourth International Neutron Transmutation Doping Conference, National Bureau of Standards, June 1-3 (1982).

23. H. Herzer and F.G. Vieweg-Gutberlet, "The Development of the Market for Neutron Transmutation Doped Silicon," Froceedings of the Fourth International Neutron Transmutation Doping Conference, National Bureau of Standards, June 1-3 (1982).

24. P.F. Kane and G.B. Larrabee, Characterization of Semiconductor Materials, McGraw-Hill Publ. Co. (1970).

25. J.N. Zemel, Nondestructive Evaluation of Semiconductor Materials and Devices, Plenum Press, New York (1979).

26. L.J. Van der Pauw, "Phillips Res. Reports," 13, 1 (1958).

27. M.G. Buehler and J.M. David, Nat'l Bureau of Stds., Special Publ. 400-29, 64 (1967).

28. Resistivity measurements of NTD samples with $9 \times 10^{15} cm^{-3} < [Ga] \leq 5 \times 10^{16} cm^{-3}$ down to 0.3 K, were done by E. Kreysa, Max Planck Institut fur Radioastronomie, Germany.

29. Lake Shore Cryotronics, Model DT-500P-GR-M, 64 E. Walnut St., Westerville, Ohio 43081.

30. G. Busch and H. Labhart, "Helv. Phys. Acta.," 19, 463 (1946).

31. A. Miller and E. Abrahams, "Phys. Rev.," 120, 1, 745 (1960).

32. N.F. Mott, "J. Non-Crystalline Solids," 1, 1 (1968).

33. E.M. Hamilton, "Phil. Mag.," 26, 1043 (1972).

34. A.L. Efros, "J. Phys. C.," 9, 2021 (1976).

35. D. Redfield, "Phys. Rev. Lett.," 30, 1319 (1973).

36. C.J. Summers and S. Zwerdling, "IEEE Trans. Microwave Theory and Tech.," MTT-22, 1009 (1974).